JOURNAL OF MAGNETIC RESONANCE **135,** 310–333 (1998)
ARTICLE NO. MN981584

DNA Duplex Dynamics: NMR Relaxation Studies of a Decamer with Uniformly ^{13}C-Labeled Purine Nucleotides

Chojiro Kojima,* Akira Ono,† Masatsune Kainosho,† and Thomas L. James*,[1]

*Department of Pharmaceutical Chemistry, University of California, San Francisco, California 94143-0446; and †Department of Chemistry, Faculty of Science, Tokyo Metropolitan University, Hachioji, Tokyo 192-03, Japan

Received May 28, 1998; revised August 21, 1998

Dynamics in a DNA decamer duplex, *d*(CATTTGCATC) · *d*(GATGCAAATG), were investigated via a detailed ^{13}C NMR relaxation study. Every 2′-deoxyadenosine and 2′-deoxyguanidine was chemically enriched with 15% ^{13}C and 98% ^{15}N isotopes. Six nuclear relaxation parameters [$R(^{13}C_z)$, $R(^{1}H_z)$, $R(2^{1}H_z{}^{13}C_z)$, $R(^{13}C_x)$, $R(2^{1}H_z{}^{13}C_x)$ and steady-state $^{13}C\{^{1}H\}$ NOE] were measured at 600 MHz and three were measured at 500 MHz (^{1}H frequency) for the CH spin systems of sugar 1′, 3′, and 4′ as well as base 8 and 2 positions. A dependence of relaxation parameter values on chemical position was clearly observed; however, no sequence-specific variation was readily evident within our experimental error of ~5–10%, except for 3′ and 5′ termini. It was demonstrated that the random 15% ^{13}C enrichment effectively suppressed both scalar and dipolar contributions of the neighboring carbons and protons on the relaxation parameters. To analyze dynamics via all observed relaxation parameters, full spectral density mapping (1992, J. W. Peng and G. Wagner, *J. Magn. Reson.* 98, 308) and the "model-free" approach (1982, Lipari and Szabo, *J. Am. Chem. Soc.* 104, 4546) were applied complementarily. A linear correlation between three spectral density values, $J(\omega_C)$, $J(\omega_H - \omega_C)$, and $J(\omega_H + \omega_C)$ was observed in plots containing all measured values, but not for the other spectral density terms including $J(0)$. These linear correlations reflect the effect of overall motion and similar internal motions for each CH vector in the decamer. The correlations yielded two correlation times, 3–4 ns and 10–200 ps. One value, 3–4 ns, corresponds to the value of 3.3 ns obtained for the overall isotropic tumbling correlation time determined from analysis of ^{13}C T1/T2 ratios. The possibility of overall anisotropic tumbling was examined, but statistical analysis showed no advantage over the assumption of simple isotropic tumbling. Lack of correlations entailing $J(0)$ implies that a relatively slow chemical exchange contributes to yielding of effective $J_{eff}(0)$ values. Based on spectral density mapping and the T1/T2 ratio analysis, three basic assumptions were initially employed (and subsequently justified) for the model-free calculation: isotropic overall tumbling, one internal motion, and the presence of chemical exchange terms. Except for terminal residues, the order parameter S^2 and the corresponding fast internal motion correlation time were determined to be about 0.8 ± 0.1 and 20 ± 20 ps, respectively, for the various CH vectors. Only a few differences were observed between or within sugars and bases. The internal motion is very fast (ps–ns time scale) and its amplitude restricted; e.g., assuming a simple wobble-in-a-cone model, the internal motion is restricted to an angular amplitude of ±22.5° for each of the 1′, 3′, 4′, 2, and 8 positions in the purine nucleotides in the entire duplex. © 1998 Academic Press

Key Words: **molecular motion; spectral density mapping; model-free analysis; wobble-in-a-cone model; order parameter; internal motion; purine chemical shift anisotropy.**

INTRODUCTION

Developments in NMR have enabled structure determination of DNA oligomers in solution (*1*, *2*). Over the course of the past decade, the quality of the structures determined has steadily improved. However, with current methods, NMR restraints obtained from dynamic molecules in solution are used in structure refinement to yield a single structure. As a result, the single structure determined cannot satisfy all experimental restraints. This conflict has been frequently observed in DNA oligomer studies (*3*, *4*), because DNA is a molecule with internal motions (*5*, *6*). Numerical approaches, such as the use of time-averaged restraints (*7*, *8*) and the probability distribution of a conformational ensemble (*4*), have been used successfully to explain the experimental restraints, nuclear Overhauser effect (NOE) intensities, and scalar coupling constants, which are time- and ensemble-averaged, i.e., compromised by conformational averaging (internal motion). However, the conformational ensembles described by numerical methods are not unique; we deal with an under-determined problem with the number of experimental observables (NOE intensities and scalar coupling constants) inadequate to define rigorously multiple (even two) interconverting structures. We can improve our approximate description of the true dynamic nature of a structure with additional experimental data, especially data that elucidate the internal motions. Strictly speaking, knowledge of the amplitude and frequency of internal motions (or conformational jumps) is necessary to describe a molecule's dynamic structure.

DNA flexibility has been studied by several physicochemical techniques (*9*, *10*). Most research has focused on the overall

[1] To whom correspondence should be addressed. Fax: (415) 502-4690, E-mail: james@picasso.ucsf.edu.

1090-7807/98 $25.00

motion, e.g., isotropic or anisotropic tumbling, and on large-scale segmental motion, i.e., bending and twisting. Consequently, we can easily estimate the isotropic correlation time of a DNA oligomer as a function of the number of base pairs (*11, 12*). In addition, some information about fast site-specific motions in DNA has been acquired via ^{13}C relaxation parameters at natural abundance (*13, 14*) or initial NOE buildup rates of specific ^{1}H–^{1}H pairs at fixed distances (*15–17*). The precision of the experimental data in those studies was not high, but their conclusions are basically in agreement: sequence-specific differences in dynamics is small except for terminal residues, and the amplitude of the internal fast motion is fairly small for both base and sugar. They are also consistent with the results from solid-state ^{2}H NMR (*9*). ^{2}H NMR gives more detailed information about fast local motions because, at very low relative humidity, overall tumbling does not affect ^{2}H T1 values and lineshapes. For example, amplitudes of fast local motions are estimated to be in the order H8 $<$ H6 $<$ H2″ $<$ H5′/H5″ for $d(CGCGAATTCGCG)_2$ in the solid state (*18*). Similarly detailed information is difficult to discern for DNA in solution without advanced techniques such as a $^{2}H/^{13}C/^{15}N$ stable isotope enrichment and heteronuclear pulse techniques.

Heteronuclear NMR techniques have dramatically developed in the last decade, enabling more accurate determination of the frequency and amplitude of overall tumbling and internal fluctuations, especially for proteins (*19–22*). They are based on ^{1}H-detected $^{2}H/^{13}C/^{15}N$ relaxation parameter measurement and analysis; the methods are applicable to DNA, but $^{2}H/^{13}C/^{15}N$ isotope enrichment is required. High-level, uniform ^{13}C enrichment introduces the complication of cross-relaxation (*23*) which is difficult to analyze. If an atom-site specifically enriched sample is available, it will give the most accurate results. Such DNA samples are available with labeling at several positions: C6 of thymidine (*24*), methyl carbon of thymidine (*25*), C1′ (*26*) and C5′ (*27*). Two of them have already been used for oligomer dynamic studies, C6 of thymidine (*28*) and C1′ (*29*). Their relaxation data are precise enough to assess several motional models, and one study reported sequence-dependent dynamics at the C1′ position (*29*). However, to elucidate internal fluctuations within a molecule thoroughly, low-level uniform labeling may be the only way to obtain sufficient sensitivity while minimizing interactions with the nearest ^{13}C nuclei (*30*).

All NMR relaxation parameters of a biomolecule in solution are determined by a spectral density function $J(\omega)$ which has attributes of overall and internal motions. Several analytical formulas of the spectral density function have been written based on various dynamic models (*5, 31*). Most internal motion models implicate the amplitude and frequency of the assumed fast internal motion model. Lipari and Szabo (*32*) presented a "model-free" approach, used in most recent NMR relaxation studies, where the amplitude and frequency of the fast internal motion is related to a generalized order parameter S and an internal motion correlation time τ_i, respectively, without specifying exactly what the motion is. Using these two parameters, the formula for the spectral density function becomes relatively simple. In a contrasting approach, Peng and Wagner demonstrated that the spectral density function itself can be mapped experimentally at several frequencies by measuring several relaxation parameters (*21*). This spectral density mapping method needs many relaxation parameters but the final results are independent of any particular dynamic model or assumptions and has several merits. For example, in protein studies, slow exchange processes are identified by an increase in the effective $J(0)$ with spectrometer field strength (*33*). For protein ^{1}H–^{15}N systems, a reduced spectral density mapping method is also available to obtain three spectral density values from three observed relaxation parameters (*34, 35*), although it is risky to apply it to ^{1}H–^{13}C systems. Using both the model-free and the spectral density mapping methods can enhance our perspective of molecular dynamics.

In the study reported here, many ^{13}C relaxation parameters were analyzed for a DNA decamer duplex in which every adenosine and guanidine is randomly fractionally enriched with 15% ^{13}C and 98% ^{15}N isotopes. The oligomer *d*(CATTTGCATC) · *d*(GATGCAAATG) was selected, because its time-averaged structure has been well characterized (*36, 37*). Refinement using restrained molecular dynamics (rMD) yields a time-averaged structure which may vary only slightly from the major conformer present in solution. It will be noted, however, that proton–proton coupling constant data suggested that most of the sugar rings possessed at least one minor conformer with altered pucker, implying that interconversion (internal motion) between the different conformers must occur. Here we will address two questions. (a) How can we determine ^{13}C relaxation parameters for individual atoms in a DNA duplex? This entails some difficult problems, e.g., relaxation analysis of methylene (*38*) and ^{13}C–^{13}C (*23*) spin systems. Here we analyze CH spin systems of sugar 1′, 3′, 4′ and base 8, 2 positions, but not the CH_2 methylenes of deoxyribose 2′ and 5′ to avoid the difficulty of the methylene relaxation and peak overlap. The effect of neighboring carbons on relaxation is shown experimentally and theoretically to be negligible because of the 15% ^{13}C enrichment. (b) Is there any sequence dependence or atomic position specificity manifest in the fast local motion? Any difference between sugar and base dynamics would certainly be of interest. Both full spectral density mapping and model-free methods are used to answer this question. Spectral density values and model-free parameters are also considered in the context of sugar repuckering inferred by previously reported scalar coupling data (*36*).

THEORETICAL BACKGROUND

Spectral Density Mapping per Peng and Wagner

From semi-classical relaxation theory (*39, 40*), each relaxation rate constant can be expressed by a linear combination

of spectral density function terms sampled at some specified Larmor frequencies of the spin system. The spectral density function is the frequency spectrum corresponding to the Fourier transform of a time-correlation function of the local magnetic field which fluctuates due to motions of the molecule containing the nuclear spins. The combination of spectral density function terms depends on the relaxation mechanism and on the spin coherence order. For CH spin systems, the primary relaxation mechanisms are due to heteronuclear dipole–dipole (DD) interactions and the chemical shift anisotropy (CSA) of the ^{13}C nucleus. By analogy with the ^{1}H–^{15}N system (*21*), one set of six measured relaxation rates[2] $R(^{13}C_z)$, $R(^{13}C_x)$, $R(^{1}H_z \rightarrow {}^{13}C_z)$, $R(2^{1}H_z{}^{13}C_z)$, $R(2^{1}H_z{}^{13}C_x)$, and $R(^{1}H_z)$ allows numerical calculation of the spectral density terms $J(\omega)$ in the right column matrix via the equation

$$\begin{pmatrix} R(C_z) \\ R(C_x) \\ R(H_z \rightarrow C_z) \\ R(2H_zC_z) \\ R(2H_zC_x) \\ R(H_z) \end{pmatrix} = \begin{pmatrix} 0 & E & D & 0 & 6D & 0 \\ 2E/3 & E/2 & D/2 & 3D & 3D & 0 \\ 0 & 0 & -D & 0 & 6D & 0 \\ 0 & E & 0 & 3D & 0 & 1 \\ 2E/3 & E/2 & D/2 & 0 & 3D & 1 \\ 0 & 0 & D & 3D & 6D & 1 \end{pmatrix} \times \begin{pmatrix} J(0) + \lambda R_{ex} \\ J(\omega_C) \\ J(\omega_H - \omega_C) \\ J(\omega_H) \\ J(\omega_H + \omega_C) \\ \rho_{H^cH^i} \end{pmatrix}, \quad [1]$$

where $D = (\mu_0/4\pi)^2 h^2 \gamma_H^2 \gamma_C^2 / 4r_{CH}^6$, $C = \Delta^2 \omega_C^2/3$, $E = 3D + C$, and $\lambda = 3/2E$. $\rho_{H^cH^i}$ is the contribution to the longitudinal relaxation rate of a given proton H^C due to all other protons H^i. Values for each physical constant are $\mu_0 = 4\pi \times 10^{-7}$ N A^{-2}, $h = 1.055 \times 10^{-34}$ N m s, $\gamma_H = 26.752 \times 10^7$ rad T^{-1} s^{-1}, $\gamma_C = 6.728 \times 10^7$ rad T^{-1} s^{-1}, and 1 T = 1 N A^{-1} m^{-1}. The internuclear ^{13}C–^{1}H bond length, r_{CH}, and ^{13}C chemical shift anisotropy Δ ($=\sigma_\parallel - \sigma_\perp$) were assumed to be constant with values of $r_{CH} = 1.096$ and 1.084 Å for sugar and base, respectively (*41*), and $|\sigma_\parallel - \sigma_\perp| = 40$ (*42*), 150 and 161 ppm for sugar, C8, and C2, respectively. CSA values for C8 and C2 were obtained minimizing the difference between experimental and simulated data based on the model-free parameters (*vide infra*). The constant D becomes 5.20×10^9 and 5.56×10^9 (rad/s)^2 for sugar and base, respectively. C becomes 0.48×10^9, 6.30×10^9, and 7.20×10^9 (rad/s)^2 at 14.1 T, and 0.33×10^9, 4.38×10^9, and 5.00×10^9 (rad/s)^2 at 11.74 T, for sugar, C8, and C2, respectively. The steady-state heteronuclear NOE is related to the cross-relaxation rate $R(^{1}H_z \rightarrow {}^{13}C_z)$ and ^{13}C longitudinal relaxation rate $R(^{13}C_z)$ via the equation (*39*)

$$\text{NOE} = 1 + \frac{\gamma_H}{\gamma_C} \frac{R(H_z \rightarrow C_z)}{R(C_z)}. \quad [2]$$

In the ^{1}H–^{13}C spin system of macromolecules, the cross-relaxation rate $R(^{1}H_z \rightarrow {}^{13}C_z)$ is very slow, typically less than 0.1 Hz, and hardly obtained with high precision. Thus experimentally the steady-state heteronuclear NOE is preferred. For this study, the heteronuclear NOE was used instead of the cross-relaxation rate itself, so the expression of $R(^{1}H_z \rightarrow {}^{13}C_z)$ in Eq. [1] was replaced with NOE and $R(^{13}C_z)$ via Eq. [2].

While the above relaxation rates essentially depend on fast molecular motions, conformational fluctuations on the time scale of microseconds to milliseconds can affect transverse relaxation rates. Fluctuations on this time scale are historically considered to be chemical exchange.The term R_{ex} reflects the contribution of chemical exchange effects to the transverse relaxation rates, $R(^{13}C_x)$ and $R(2^{1}H_z{}^{13}C_x)$. $R_{ex} = \pi * L$, where L is the conventional exchange broadening observed in spectral peaks when a molecule is undergoing "fast exchange" (*33, 43*). In most applications of spectral density mapping, $J(0)$ includes the chemical exchange term because it is difficult to distinguish the real $J(0)$ value from the apparent one. This effective $J(0)$ value was used originally (*21*) but, as suggested recently (*33*), it will be convenient to call this old-style term $J_{eff}(0)$,

$$J_{eff}(0) = J(0) + \lambda R_{ex}, \quad [3]$$

where λ is defined in Eq. [1]. The chemical exchange contribution to $J_{eff}(0)$ may be determined by the use of multiple field strengths (*33*). $J(0)$ does not depend on the magnetic field strength, but the exchange process may be proportional to the square of the ^{13}C Larmor frequency. In other words, $J_{eff}(0)$ increases with the square of the spectrometer field strength but $J(0)$ does not, so measurements at two or more magnetic field strengths may enable discernment of the exchange contribution by spectral density mapping.

Model-Free Approach of Lipari and Szabo

The spectral density function is calculated from an autocorrelation function describing the time dependence of the orientation of a nucleus (CSA mechanism) or a vector connecting two nuclei (DD mechanism); the orientation is conveniently expressed as a Wigner rotation matrix element. The correlation function is a simple exponentially decaying function in solution, primarily due to random motion of the whole molecule originating from collisions with solvent or other solute molecules and secondarily from local motions within the molecule. Each of the overall and internal motions can be independently expressed as a random process. Random motion, i.e., Mark-

[2] The relaxation rates are $R(^{13}C_z)$, ^{13}C spin–lattice relaxation rate; $R(^{13}C_x)$, ^{13}C transverse relaxation of in-phase coherence; $R(^{1}H_z \rightarrow {}^{13}C_z)$, heteronuclear cross-relaxation rate; $R(2^{1}H_z{}^{13}C_z)$, ^{13}C longitudinal two-spin order relaxation rate; $R(2^{1}H_z{}^{13}C_x)$, transverse relaxation of antiphase coherence; and $R(^{1}H_z)$, spin–lattice relaxation rate of the carbon-bound proton.

ovian or Brownian motion, is physically characterized by exponential decay of the correlation function, so the individual correlation function is exponential. Lipari and Szabo defined a limiting value, at very long times, of the internal motion correlation function as the square of the generalized order parameter S (*32*). The term "order parameter" has been used in the literature to designate both S and S^2. As that is confusing, in this report S^2 or S is explicitly written together with the term "order parameter."

If overall and internal motions are assumed to be independent, the total correlation function may be written as a simple product of the overall and internal correlation functions. In the simplest approximation, overall and internal motions can be described respectively by single correlation times, τ_o and τ_i, and the total correlation function $C(t)$ and spectral density $J(\omega)$ are (*32*)

$$C(t) = \left(\frac{1}{5}\, e^{-t/\tau_o}\right)(S^2 + (1 - S^2)e^{-t/\tau_i}) \qquad [4]$$

$$J(\omega) = \frac{2}{5}\left(S^2\, \frac{\tau_o}{1 + (\omega\tau_o)^2} + (1 - S^2)\, \frac{\tau}{1 + (\omega\tau)^2}\right), \qquad [5]$$

where $\tau^{-1} = \tau_o^{-1} + \tau_i^{-1}$. The precise form of a correlation function depends on the nature of the molecular motions (*5, 31*). Lipari and Szabo do not specify any particular motional model, so just the exponentials are used as a correlation function. As a result, the model-free approach does not have a concrete physical picture of the molecular motion, but does have a simple form to relate with most physical models. Note that Eqs. [4] and [5] are the simplest forms of the model-free approach; more complicated forms can be generated if additional internal motions or significantly anisotropic overall tumbling are considered.

As evident in Eq. [5], three model-free parameters are requisite and sufficient to create a spectral density function, i.e., overall correlation time τ_o, internal correlation time τ_i, and order parameter S^2. Subsequently, most relaxation parameters can be simulated by five spectral density values as shown Eq. [1]. However, two additional parameters, the exchange contribution R_{ex} and the proton–proton longitudinal relaxation rate $\rho_{H^cH^i}$, are also required for generation of all six relaxation parameters. R_{ex} and $\rho_{H^cH^i}$ may depend on the measured magnetic field strength (*33*), so different values of R_{ex} and $\rho_{H^cH^i}$ are assumed at different field strengths.

METHODS AND MATERIALS

Preparation of the DNA Oligonucleotides

The basic approach to preparation of the labeled DNA oligomers has been described (*44*). The 15% ^{13}C- and 98% ^{15}N-enriched adenosine and guanidine was prepared using reported methods (*45, 46*) with minor modifications (Japanese Patent No. 4-52118, 1992): *Bacillus subtilis* was used instead of *Escherichia coli* with randomly fractionally labeled 15% [^{13}C]glucose and 98% $^{15}NH_4Cl$ as the sole source of carbon and nitrogen. The labeled nucleoside was chemically converted to the 2′-deoxy form (*47*) and subsequently its 3′-phosphoramidite (*48*), which was used for oligonucleotide synthesis on a DNA synthesizer (Applied Biosystems Inc., ABI 392). The two fully protected and labeled DNA strands, *d*(CATTTGCATC) and *d*(GATGCAAATG), were deblocked and purified by the conventional C18 HPLC column procedure (*49*). Every purine was enriched with ^{13}C and ^{15}N, but pyrimidines were not. Final purity of the oligomers was >95% by C18 HPLC. The 1:1 stoichiometry necessary for duplex formation was determined by adding aliquots of one decamer to a solution of the complementary strand oligomer while monitoring with UV spectroscopy. No peak corresponding to single-strand oligonucleotide was observed for the final DNA solution in the NMR spectrum. The NMR sample was dissolved in 230 μl of 20 m*M* phosphate buffer containing 100 m*M* NaCl and 0.1 m*M* EDTA, adjusted to pH 6.8, lyophilized and dissolved in D_2O. The resulting solution was degassed and kept in a 5 mm microtube (Shigemi Inc., Tokyo). The concentration was estimated to be 0.9 m*M* double-strand by UV absorbance using the absorptivity calculated from the nearest neighbor approximation method (e.g., (*50*)).

NMR Spectroscopy[3]

All NMR spectra were recorded at 30°C on a Varian UNITYplus 600 MHz spectrometer or a GE Omega 500 MHz spectrometer with triple-resonance probes. The UNITYplus was equipped with a unit enabling pulsed field gradients along the z axis, but the Omega was not. By utilizing earlier ^{1}H resonance assignments at 25°C (*36*), ^{13}C assignments were made on 2D ^{13}C–^{1}H heteronuclear single quantum coherence (HSQC) correlation spectra followed by a HSQC–NOESY spectrum (*51*). Assuming $J_{CH} \approx 6$–28 Hz, long-range HSQC spectra were also recorded to correlate the adenine H2 and H8 resonances. Five auto-relaxation rate constants and one heteronuclear NOE were measured for the C–H spin systems of deoxyribose 1′, 3′, and 4′ and base 8 and 2 positions. The longitudinal ^{13}C relaxation rate $R(^{13}C_z)$, the longitudinal proton spin–lattice relaxation rate $R(^1H_z)$ and the longitudinal two-spin order relaxation rate $R(2^1H_z{}^{13}C_z)$ were each measured at two magnetic field strengths—14.1 T (600 MHz ^{1}H frequency) and 11.74 T (500 MHz ^{1}H frequency). The in-phase ^{13}C transverse relaxation rate $R(^{13}C_x)$, the antiphase ^{13}C transverse relaxation rate $R(2^1H_z{}^{13}C_x)$ and the steady-state ^{13}C–^{1}H NOE were determined at 600 MHz ^{1}H frequency only due to the low sensitivity of our 500 MHz spectrometer.

The relaxation rates were measured in a series of 2D heteronuclear ^{13}C–^{1}H correlated spectra using an INEPT and a reverse INEPT to enhance sensitivity. Details of the pulse

[3] Pulse sequences and parameters are available from the authors.

sequences were described previously (*21, 23*). For all 600 MHz experiments, several magnetic field gradient pulses were added to eliminate noise. These gradient pulses suppressed the water signal so well that presaturation was not used. The ^{13}C pulse field strength was 2.3 kHz (90° pulse width ~110 μs) for the continuous-wave ^{13}C spin-lock for $R(^{13}C_x)$ and $R(2^1H_z{}^{13}C_x)$ measurements at 600 MHz ^1H frequency. Quadrature detection in t1 was utilized via the States–TPPI method (*52*). To enhance digital resolution and avoid heating during decoupling while measuring each relaxation parameter, ^{13}C–^1H correlated spectra of the deoxyribose 1′, 3′, and 4′ (^{13}C shifts of ~78–90 ppm) and the base 2 and 8 nuclei (^{13}C shifts of ~122–144 ppm) were separately acquired as their chemical shifts differ substantially. Each 2D spectrum consisted of 64 or 128 increments in the ^{13}C dimension with 2048 complex points per FID, and spectral widths for ^1H, ^{13}C sugar and ^{13}C base of 4000, 1500, and 2500 Hz at 500 MHz ^1H frequency, and 5000, 1800, and 3300 Hz at 600 MHz ^1H frequency, respectively. The pulse repetition time was 1.5 s, i.e., ~3 times ^{13}C T1, and the total acquisition time of each 2D spectrum was 7, 3.5, and 1.7 h for ^{13}C–^1H NOE, $R(^{13}C_z)$, and other experiments, respectively. Each relaxation data set was recorded with the following relaxation delay times—$R(^{13}C_z)$: 30, 60, 90, 120, 200, 300, 400, 500, 750, 1000, 1500, and 3000 ms at 600 MHz ^1H frequency, and 30, 60, 90, 120, 150, 200, 250, 300, 600, 900, 1200, and 1500 ms at 500 MHz ^1H frequency; $R(^1H_z)$: 40, 80, 120, 160, 200, 250, and 300 ms; $R(2^1H_z{}^{13}C_z)$: 40, 80, 120, 160, 200, 250, and 300 ms; $R(^{13}C_x)$: 8, 17, 25, 34, 51, and 68 ms at 600 MHz ^1H frequency; $R(2^1H_z{}^{13}C_x)$: 5, 10, 15, 20, 25, 30, 40, 50, and 60 ms at 600 MHz ^1H frequency. Steady-state ^{13}C–^1H NOE values were acquired with three spectra recorded with 3 s of proton saturation and three others without proton saturation. The total acquisition time for the ^{13}C–^1H NOE and $R(^{13}C_z)$ experiments was 2 days, and 1 day was required for the other experiments.

The in-phase ^{13}C transverse relaxation rate $R(^{13}C_x)$ was determined three times using three different pulse sequences. The two-pulse spin echo sequence, the Carr–Purcell–Meiboom–Gill (CPMG) sequence, 90°_x–$(-\Delta-180^\circ_y-\Delta-)_{2n}$–, and the PERFECT sequence (*53*), 90°_x–$(-\Delta-180^\circ_y-\Delta-90^\circ_y-\Delta-180^\circ_y-\Delta-)_n$–, were used instead of a continuous wave spin-lock to elucidate the effects of the ^{13}C–^{13}C scalar coupling on $R(^{13}C_x)$ measurements with the following relaxation delay times Δ: 4, 12, 21, 37, 53, 70, and 86 ms at 600 MHz. Pulse field strengths of the spin echo sequences were 20 and 3.7 kHz for CPMG and 20 kHz for PERFECT; these values were determined by a 90° pulse width at each pulse power level within a 5% precision. The PERFECT sequence can refocus the two-spin homonuclear scalar coupling terms, e.g., ^{13}C–^{13}C two-spin coherence.

NMR Data Processing and Relaxation Parameter Analysis

All 2D NMR spectra were processed on Sun Sparcstation 2 or Silicon Graphics Inc. IRIS Indigo R5000 workstations using the software nmrPipe (NIH, Bethesda) (*54*) and our locally written SPARKY (see http://picasso.ucsf.edu/software.html). A 90°-shifted sine-squared window function was applied in the t2 dimension and a 90°-shifted sine window function was applied in the t1 dimension. Each dimension was zero-filled twice prior to Fourier transformation.

The Levenberg–Marquardt algorithm for least squares fitting, utilizing KaleidaGraph 3.0 (Abelbeck Software), was used to extract relaxation rate constants assuming a monoexponential decay of cross-peak intensities. Three-parameter fitting ($y = A - Be^{-Cx}$) was applied to $R(^{13}C_z)$, but two-parameter fitting was employed ($y = Ae^{-Bx}$) for the other relaxation data. Intensities were taken from peak heights instead of peak volumes, because there is no difference between the peak height and volume methods with linewidths unchanged and experimental intensity errors are easily defined by the peak height method. Moreover peak volume integration for small peaks is time-consuming and unreliable. The uncertainty in the measured height was assumed to be the standard deviation of the spectral noise. Experimental errors in the determined rates were obtained from the error matrices of the nonlinear least squares fitting to single exponential functions. For steady-state NOE values, the error was computed by simple error propagation based on peak height uncertainties.

Full spectral density mapping was applied at 600 MHz ^1H frequency following the protocol of Peng and Wagner (*21*). Five relaxation rates and one steady-state NOE were converted to five spectral density values at five different frequencies and one proton–proton longitudinal relaxation rate $\rho_{H^cH^i}$ (Eqs. [1] and [2]). The exchange contribution was not separated, so at 0 MHz, $J_{\text{eff}}(0)$ (defined by Eq. [3]) was determined, not $J(0)$. At 500 MHz, only three relaxation parameter measurements were made due to low sensitivity. These three relaxation rates were converted to just one spectral density value at $\omega_C = 125$ MHz, $J(125)$. Errors for $J(\omega)$ and $\rho_{H^cH^i}$ values were estimated by a Monte Carlo procedure. Experimental relaxation parameters and their estimated errors were assumed to be the means and variances of a Gaussian distribution. From each such distribution, 100 synthetic relaxation data sets were created. Calculation of $J(\omega)$ and $\rho_{H^cH^i}$ values was performed for each of the 100 synthetic relaxation data sets. The standard deviations of the resulting ensemble of $J(\omega)$ and $\rho_{H^cH^i}$ values were taken as the estimated errors. One hundred synthetic data sets may be enough to estimate errors because a simple error propagation procedure gave similar results, and moreover 200–1000 data sets were generated for some residues but the resulting errors were similar to that of only 100.

With minor modifications, model-free parameters were obtained as previously described (*20*). To find the best model-free parameters, we minimized χ^2,

$$\chi^2 = \frac{1}{n}\sum_{i=1}^{n}\left(\frac{(R_i(\text{obs}) - R_i(\text{calc}))^2}{\sigma_i^2}\right), \qquad [6]$$

where R_i(obs) and R_i(calc) were the ith observed and calculated relaxation parameters, and σ_i was the estimated error of the ith observed relaxation parameter. The overall correlation time τ_o was determined by χ^2 minimization of the ^{13}C T1/T2 ratio ($=R(^{13}C_x)/R(^{13}C_z)$) assuming $S^2 = 1$. As suggested previously (*20*), the T1/T2 ratio was assumed to be approximately independent of τ_i and S^2; overall correlation time values were thus calculated for each labeled site in the duplex, and these values were averaged. The other five model-free parameters, namely τ_i, S^2, R_{ex}, $\rho_{H^cH^i}$ at 500 MHz and $\rho_{H^cH^i}$ at 600 MHz, were determined by χ^2 minimization of all observed relaxation parameters with a fixed τ_o value which was determined by the T1/T2 ratio method. Errors for model-free parameters were also estimated by a Monte Carlo procedure using 100 synthetic data sets as described above for spectral density mapping. For most calculations, including spectral density mapping, Microsoft Excel 5.0 (Microsoft Corp.) was used with the solver add-in function and the Visual Basic-based macroprogram.

RESULTS AND DISCUSSION

^{1}H–^{13}C Correlation Spectra and ^{13}C Resonance Assignments

Two-dimensional ^{1}H–^{13}C correlation spectra of the DNA decamer were recorded with a refocused-HSQC pulse sequence. Each sugar and base spectral region is shown with peak assignments in Fig. 1(upper and lower, respectively). The constant time procedure was not used here, but no obvious ^{13}C–^{13}C coupling appeared in 2 h of spectral acquisition. ^{13}C assignments were based on previous ^{1}H assignments at 25°C (*36*); most 1′ and aromatic resonances were easily assigned, considering a slight shift due to the temperature difference (30°C in this report). Most 3′ and some other peaks were not assigned due to overlapping ^{1}H chemical shifts. To solve this problem, HSQC–NOESY and long-range HSQC spectra were acquired. Most intraresidue NOESY cross-peaks including 1′, 2′, 2″, 3′, and 4′ resonances, and all adenine H2–H8 scalar correlation peaks through C4 were identified. As a result, all CH signals were assigned. Most peaks, except five shown in Fig. 1, were well separated though these resonances emanate only from purine residues. ^{13}C chemical shift values for sugar carbons were typical of B-DNA, i.e., for the 2′-*endo* sugar conformation (*55*).

Over the time period (~1000 h) of this NMR study conducted at 30°C, signals entailing all H8 and H2 protons were qualitatively observed to decrease due to exchange with solvent deuterium (*56*). The exchange rate of guanosine H8 was dependent on the sequence, where that of the 5′-terminal residue (G11) was relatively fast (half-life of ~500 h compared to ≥1000 h for others). At high temperature, several hours were sufficient to observe exchange; e.g., to recover aromatic proton signals, the duplex was heated to ~80°C for ~3 h. The order of the exchange rate was guanosine H8 (fast) > adenosine H8 (intermediate) > adenosine H2 (slow). The sequence dependence was obvious only for guanine H8 and not clear for the others within 1000 h (see Fig. 1). For the four guanine H8 protons, the order of the exchange rate was G11 ≫ G6 > G14, G20. G11 is the 5′-terminal residue, and G6 is at the kinked position in the sequence (*37*). Based on the proposed exchange mechanism (*56*), such relative exchange rates would depend on accessibility of water to the N7–C8 bond; i.e., both G11 and G6 would be accessible to water. However, the water accessibility is not sufficient to explain everything; for example, the 3′-terminal residue G20 should be accessible to water, but its exchange rate is slow. These exchange rates may depend on both water accessibility and nucleic acid structure, because the nucleic acid's structure can shift base pK_a values (*57*). More detailed theoretical and experimental studies will be necessary to elucidate the effect of nucleic acid structure on this exchange rate.

The long-range HSQC spectrum was used to correlate intraresidue H2 and H8 peaks through the C4 resonance. This spectrum was surprisingly sensitive for our 15% ^{13}C-enriched sample, and residual ^{13}C4–^{13}C5 doublets (ca. 60 Hz) were seen for most H2–C4 correlation peaks. Total acquisition time was less than 4 h, which was enough to identify all intraresidue H2–H8 connectivities for the 0.9 m*M* sample. The HMBC experiment was reported for 1.5 m*M* DNA of a 20-base hairpin at natural abundance to require a total acquisition time of 80 h using a 750 MHz spectrometer (*58*). These experiments should become a good tool for revealing intraresidue H2–H8 correlations; e.g., the sensitivity for a fully ^{13}C-labeled sample would be six times higher than for that of our 15% ^{13}C-enriched sample although the constant-time procedure or some other minor modification would be required.

^{13}C Relaxation Rate Contribution from Other ^{13}C Nuclei in 15% ^{13}C-Enriched DNA

The ^{13}C signal intensity in a 15% ^{13}C-enriched sample is simply expected to be 15 times higher than that for a natural abundance sample. However, when directly or nondirectly bonded ^{13}C nuclei are considered, that will not necessarily be true because of ^{13}C contributions from DD or scalar interactions. This could be a serious problem for relaxation analysis. The scalar contribution perturbs transverse relaxation rates, and DD interactions change most relaxation rates. In the following we consider how much directly and nondirectly bonded ^{13}C nuclei contribute to the relaxation rates determined.

The directly bonded ^{13}C scalar contribution is not evident in a HSQC spectrum as shown in Fig. 1. This result appears simple, but let us consider this more carefully. A randomly fractionally 15% ^{13}C-enriched DNA sample creates a very complicated carbon spin system with an array of different ^{12}C and ^{13}C nuclei. Neglecting long-range, i.e., ^{13}C–^{13}C contributions from not directly bonded ^{13}C, the fraction of each carbon spin system was computed to be 10.8% ^{12}C–^{13}C–^{12}C (singlet),

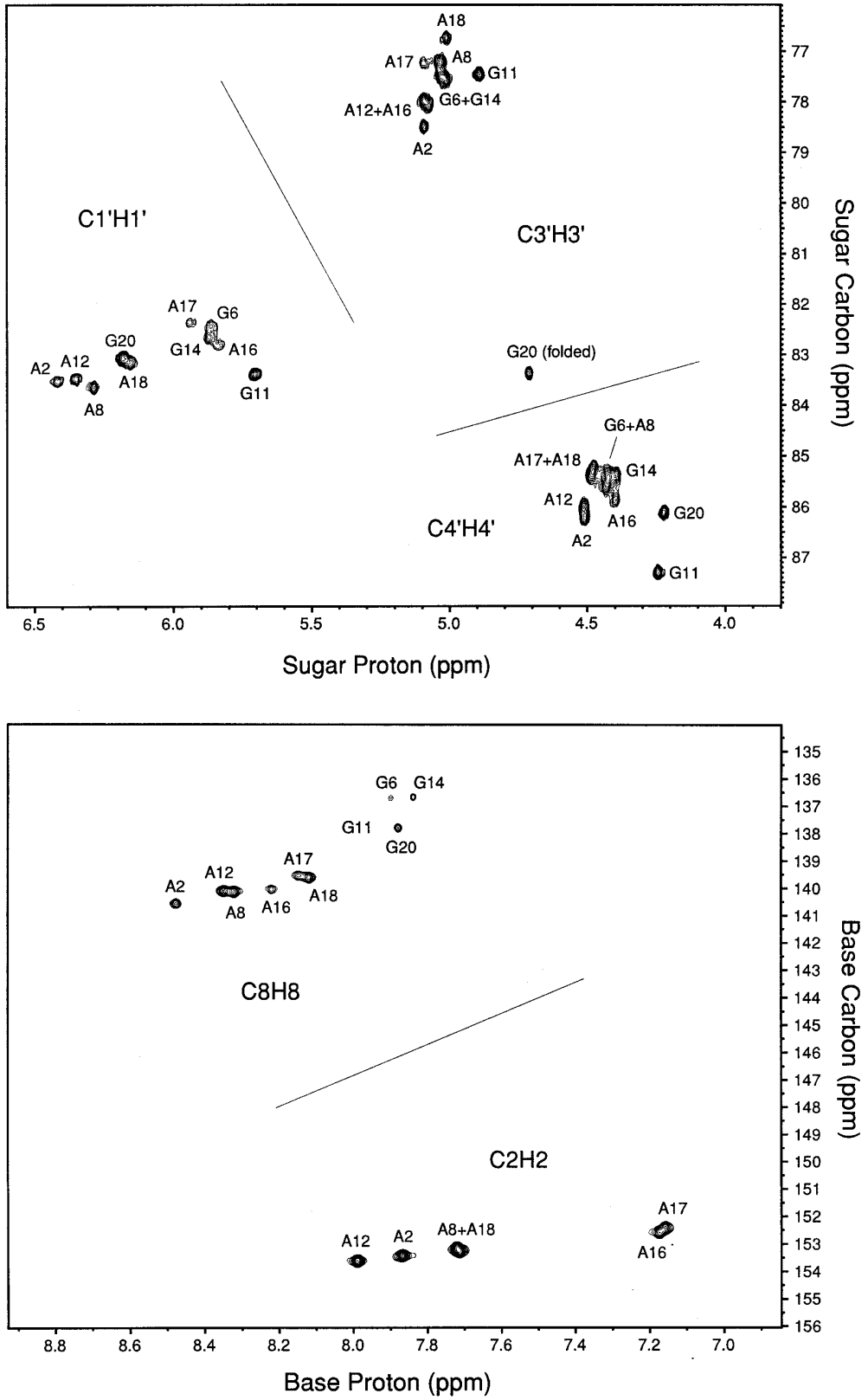

FIG. 1. ^{1}H–^{13}C heteronuclear correlation spectra for sugar (upper) and base (lower) resonances of a DNA decamer *d*(CATTTGCATC) · *d*(GATGCAAATG). The refocused-HSQC sequence was used on a Varian Unityplus spectrometer operating at a ^{1}H frequency of 600 MHz for a sample consisting of 0.9 m*M* duplex in D_2O with 20 m*M* phosphate buffer containing 100 m*M* NaCl and 0.1 m*M* EDTA (pH 6.8) at 30°C. Each 2D spectrum resulted from 64 or 128 increments

1.9% ^{12}C–^{13}C–^{13}C (doublet), 1.9% ^{13}C–^{13}C–^{12}C (doublet), and 0.3% ^{13}C–^{13}C–^{13}C (triplet). The doublet peaks are theoretically nonnegligible. Actually doublet signals were evident in a half-day of spectral accumulation, but the triplet was not. These doublets generally appear as an increase in noise. In the worst case, it could be ~2–20 times larger than the thermal noise for the typical S/N ratio of ~5–50. This perturbation could be serious for many 3′ and some 4′ signals which had similar ^{1}H chemical shifts. Most relaxation time values did not depend on the sequence, as described later; thus these residual doublet errors were manifest as an amplitude modulation, $\cos(\pi J_{CC}t)$. The maximum amplitude was estimated as a singlet/doublet ratio of 18% (1.9/10.8) or smaller depending on the degree of overlap of the doublet "noise" and the singlet signal. Most peaks in our experiments did not show this cosine modulation because the doublets were not heavily overlapping, but certain 3′ and 4′ peaks were modulated, as expected. The maximum amplitude observed was about 7–10%, which is smaller than that for the fully overlapped case. For these peaks, many relaxation rates were determined by fitting with and without the cosine modulation term, but no clear difference was found. So, while the doublet contribution is not negligible, it is not serious in most cases. Finally, we reached an important and simple conclusion about the directly bonded ^{13}C contribution in our experiments. The ^{13}C signal detected was attributed to the ^{12}C–^{13}C–^{12}C spin system and assumed to have no scalar and DD interaction with the directly bonded carbon nuclei as expected initially, because the $^1J_{CC}$ value was larger than the ^{13}C linewidth and triplets were negligible. We caution, however, that if the constant-time procedure is used in the pulse sequences employed, these merits will be lost instead of the slight signal gain usually garnered.

Long-range, i.e., more than two bonds apart, ^{13}C contributions were more complicated to assess than those for the directly bonded ^{13}C case. As above, we can safely neglect the triplet contribution. However, the indirect ^{13}C–^{13}C J coupling constant is smaller than or similar to the ^{13}C linewidth, so singlets cannot be observed separately from the doublets. Theoretically both scalar and dipolar interactions are not negligible. In the case of scalar coupling, principally transverse relaxation decay is perturbed. The PERFECT sequence can refocus the scalar coupling term of the homonuclear two-spin system (*53*), but other spin-lock or spin echo sequences cannot. In our 15% ^{13}C-enriched sample most signals were singlets or doublets, so PERFECT can refocus them. For the 15% enriched sample, the scalar coupling effect was estimated by comparing the ^{13}C transverse relaxation rates $R(^{13}C_x)$ determined by four different spin-lock or spin echo sequences: CPMG at high and low power, continuous wave (CW), and PERFECT (see Fig. S1 of Supplementary Materials placed at the authors' website: http://picasso.ucsf.edu). Though the CW sequence gave slightly slower relaxation rates, no clear pulse sequence dependence was seen. In other words, the scalar coupling effect was smaller than our experimental error. In contrast, the DD contribution was roughly estimated by the magnitude of the constant D in Eq. [1]. The only difference between directly and nondirectly bonded CH systems is the CH distance, i.e., 1.1 Å for the directly bonded system, 2.1–2.2 Å for two-bond, 2.2–3.5 Å for three-bond, and so on. In our decamer molecule, the shortest CH distance was 2.5 Å for CH pairs more than three bonds apart (*37*). So at least the D value of the nondirectly bonded CH system was $(1.1/2.1)^6 \approx 48$ times smaller than that of the directly bonded CH. However, the number of the nondirectly bonded protons could be large, so the resulting systematic error can reach 5–7% in the case of the protein Cα (*59*). This might be taken into account as a fictitious decrease of the CH distance by about 1% (*59*).

For our system, both directly and nondirectly bonded ^{13}C nuclei had a negligible effect on determination of relaxation rates. Because this conclusion is applicable only to our system, we consider the general applicability of 15% enriched samples for relaxation studies. The directly bonded ^{13}C contribution is theoretically negligible except for errors due to overlap of the dominant ^{13}C singlet signals with ^{12}C–^{13}C–^{13}C or ^{13}C–^{13}C–^{12}C doublets. This error can be eliminated by minor modifications of pulse sequences, though overlap should not be a serious problem in a relaxation study. For example, it can be minimized by changing the constant-time delay from $n/2J_{CC}$ to $1/4J_{CC} + n/2J_{CC}$, where n = integer. The scalar contribution from nondirectly bonded ^{13}C will not be serious for most macromolecules, as shown experimentally above. The DD contribution depends on the molecular structure, so CC and CH distances from carbons and protons not directly bonded should be calculated before relaxation analysis.

Relaxation Rate Measurements

Before starting our motional analysis, we wish to make sure that the observed relaxation data are free from systematic errors. Some potential errors have been pointed out for ^{1}H–^{15}N studies in proteins (for example, (*60*) and references therein). Here we consider the ^{1}H–^{13}C system in nucleic acids which are also labeled with 98% ^{15}N. First, carbon–carbon and carbon–nitrogen cross-relaxation are treated. As explained in the pre-

in the ^{13}C dimension with 2048 complex points per free induction decay (FID), with spectral widths for ^{1}H, ^{13}C sugar, and ^{13}C base of 5000, 1800, and 3300 Hz, respectively. The pulse repetition delay time was 1.5 s, and the total acquisition time was 1.7 h. The following five CH spin pairs were overlapped: C^{2}H2 (A8, A18), C3′H3′ (G6, G14), C3′H3′ (A12, A16), C4′H4′ (G6, A8), and C4′H4′ (A17, A18). The C8H8 resonance of 5′-terminal G11 was too small to be observed in this particular spectrum due to exchange with deuterium from the solvent D_2O. The C3′H3′ resonance of 3′-terminal residue G20 is folded—the real ^{13}C chemical shift is 73.2 ppm.

vious section, carbon–carbon DD cross-relaxation was negligible and the carbon–carbon scalar contribution was very small in our 15% ^{13}C-enriched sample. The magnitude of the carbon–nitrogen DD cross-relaxation was estimated by the constant D in Eq. [1]. The ratio $D(^{13}C^{1}H)/D(^{13}C^{15}N)$ is >200, where bond length r_{CN} = 1.3–1.5 Å and gyromagnetic ratio γ_N (^{15}N) = -2.712×10^7 rad T^{-1} s^{-1}. For the directly bonded CH system, carbon–nitrogen DD cross-relaxation was always negligible. On the other hand, scalar coupling constants between ^{13}C and ^{15}N range from 0 to 11 Hz as determined by Kainosho and co-workers (unpublished results). This carbon–nitrogen scalar interaction may cause systematic errors and sensitivity loss. In our experiments, the heteronuclear ^{13}C–^{15}N J coupling terms were suppressed by the spin-lock or the spin echo sequences during the transverse relaxation delay time. Consequently, both carbon–carbon and carbon–nitrogen interactions were negligible in our system. Even when ^{14}N is considered instead of ^{15}N this conclusion will not change, because the gyromagnetic ratio $\gamma_N(^{14}N) = 1.934 \times 10^7$ rad T^{-1} s^{-1} is smaller than that of ^{15}N and scalar relaxation of the second kind (^{13}C–^{14}N) is negligible for the molecule rotating with a correlation time >2 ns (*23*).

$R(^{13}C_z)$ measurement. Major error sources were proton–carbon heteronuclear DD cross-relaxation and carbon DD–CSA cross-relaxation. Both cross-relaxation contributions can be eliminated by proton saturation (*61, 62*). Here proton saturation was accomplished by two long pulses (1.0 and 0.5 ms) followed by a train of 180° pulses every 5 ms (*23*). The longitudinal ^{13}C relaxation rate was measured via inversion–recovery (IR) experiments. The NOE-type experiment (*23, 63*) was also carried out, but the results were not used in our relaxation analysis. One merit of the NOE-type experiment was the shorter acquisition time (about 1 day), half that of the IR experiment. Another merit was the number of parameters to be fitted: two and three parameters for the NOE and IR experiments, respectively. Nevertheless, the precision of fitted parameters in the NOE experiment was lower than that in IR experiments due to low signal-to-noise ratio and the maximum intensity change during the relaxation period; i.e., in the IR experiment the signal sign changes from negative to positive but in the NOE experiment it is always positive. If the S/N ratio is high enough, precision does not depend on the method of measuring. For our 0.9 mM 15% ^{13}C-enriched sample, the sensitivity was not high enough to eliminate this method dependence on fitted parameter precision.

$R(^{13}C_x)$ measurement. Potential error sources were the homo- and heteronuclear scalar interaction and the carbon DD–CSA cross-relaxation. The carbon–carbon homonuclear scalar contribution was negligible, as mentioned above. The heteronuclear J coupling interaction was effectively killed by the continuous wave spin-lock or by short spacing of pulses in spin echo sequences. Cross-relaxation can be suppressed by the proton composite 180° pulses every 4 ms within the spin-locking or the spin echo period (*61, 64*). The off-resonance contribution was evaluated according to (*65*).

$$R(^{13}C_{\rho z'}) = R(^{13}C_z)\cos^2\theta + R(^{13}C_x)\sin^2\theta, \qquad [7]$$

where θ is the tip angle of the effective field relative to the laboratory z-axis as given by the relation tan θ = (pulse field strength)/(resonance offset). The $\sin^2\theta$ values ranged from 0.75 to 1.0 under our experimental conditions, where the ^{13}C pulse field strength for spin-locking was 2.3 kHz and the spectrum width was less than 3300 Hz. In the worst case the $R(^{13}C_x)$ value had an $R(^{13}C_z)$ contribution ≈20%, although most were comparable to the experimental error (~10%) and $\sin^2\theta$ values were >0.9. These systematic errors will be recognized as negative R_{ex} values or relatively small $J_{eff}(0)$ values.

$^{13}C\{^1H\}$ NOE measurement. In general the absolute value of the steady-state ^{13}C{^{1}H} NOE is small and hardly obtained as quantitatively as the ^{15}N{^{1}H} NOE, since the value $\gamma(^1H)/\gamma(^{13}C) = 3.98$ in Eq. [2] is less than half the magnitude of $\gamma(^1H)/\gamma(^{15}N) = -9.86$. Peak intensities in an ^{15}N{^{1}H} NOE spectrum change from positive in the slow tumbling limit to negative in the fast narrowing limit, i.e., positive for rigid regions but negative for flexible regions in most proteins or nucleic acids. On the contrary, peaks in the corresponding ^{13}C spectrum are always positive, so quantitative observation of the small signal enhancement with good S/N ratio is required. This sensitivity problem has been solved by repeating the same experiment several times. The most serious problem is not the sensitivity but the long preequilibrium delay time required by the small ^{13}C{^{1}H} NOE value. For example, the preferred preequilibrium delay times were 20 and 45 s for sugar and base for our experimental conditions, where the averaged $R(^1H_z \rightarrow {}^{13}C_z)$ values were 0.15 and 0.07 rad/s for sugar and base. The $R(^1H_z \rightarrow {}^{13}C_z)$ values were estimated from Eq. [2] using averaged ^{13}C{^{1}H} NOE values and $R(^{13}C_x)$ values of 1.3 and 2.0 rad/s for sugar and 1.1 and 2.6 rad/s for base, respectively. We examined several pre-equilibrium delay times from 0.5 s to 5.0 s, and found that 3.0 s was a good choice. If the shorter delay time was used, the NOE value became smaller. If a longer delay time was used, NOE values became less reproducible due to hardware instability during the increased total acquisition time (~4 days). Assuming 10–30% underestimation of the NOE value, the $R(^1H_z \rightarrow {}^{13}C_z)$ value becomes 1.5- to 4-fold smaller. That seems consistent with our experimental results, so our NOE values may be systematically underestimated. In general, this systematic error is minimized by the long pre-equilibrium delay time but, as mentioned above, significant experimental error may occur anyway.

$R(2^1H_z{}^{13}C_z)$ and $R(2^1H_z{}^{13}C_x)$ measurement. Identified error sources were carbon DD–CSA cross-relaxation and external two-spin order induced by proton–proton DD cross-relaxation. For $R(2^1H_z{}^{13}C_x)$, the homo- and heteronuclear scalar interaction and the off-resonance contribution were addition-

ally considered but are not mentioned further here (see $R(^{13}C_x)$ measurement). Carbon DD–CSA cross-relaxation was reduced by the 180° proton pulse. Though not eliminated completely, the resulting systematic error was expected to be small because DD–CSA cross-relaxation was slow relative to the auto-relaxation rates, $R(2^1H_z{}^{13}C_z)$ and $R(2^1H_z{}^{13}C_x)$. For sugar carbons, CSA values were small (~40 ppm), and the DD–CSA cross-relaxation rate may be very slow. In contrast, for base carbons the CSA was large (~150 ppm), so the cross-relaxation rate could be fast and the resulting systematic error may not be negligible. External two-spin orders were generated by proton–proton DD cross-relaxation and experimentally not suppressed at all. The proton–proton DD cross-relaxation rate is slower than the auto-relaxation rates $R(2^1H_z{}^{13}C_z)$ and much slower than $R(2^1H_z{}^{13}C_x)$; thus the systematic error was expected to be small, especially for $R(2^1H_z{}^{13}C_x)$. Using the program CORMA, the maximum error from proton–proton DD cross-relaxation was estimated to be <10% of $R(2^1H_z{}^{13}C_z)$ for most cases but ~30% for the base 8 position. The CORMA calculation will be described later. As shown above, systematic errors were not neglected but are expected to be small.

$R(^1Hz)$ measurement. Heteronuclear DD cross-relaxation and proton–proton DD cross-relaxation are potential sources of error. The ^1H–^{13}C DD cross-relaxation rate $R(^1H_z \rightarrow {}^{13}C_z)$ was <0.2 rad/s (*vide supra*), much slower than $R(^1H_z) \approx 3$ rad/s. The slowest $R(^1H_z)$ was 0.9 rad/s found for adenosine H2, and the corresponding ^1H–^{13}C DD cross-relaxation rate was 0.07 rad/s. Always its contribution was less than 10%. The proton–proton DD cross-relaxation rate was much faster than that of ^1H–^{13}C but slower than the proton DD auto-relaxation rate. The proton–proton cross-relaxation contribution was suppressed by selective inversion of the ^{13}C-attached protons using the HSQC–NOESY sequence. The ^{13}C-attached protons in both dimensions were 2.25% of all ^{12}C- and ^{13}C-attached protons in our 15% enriched sample. At least 85% of the cross-relaxation detected in the NOESY–HSQC spectrum was suppressed in the HSQC–NOESY spectrum. Both heteronuclear and proton–proton DD cross-relaxation contributions were relatively small (15% or less) and comparable to experimental error.

Most relaxation data obtained were not free from systematic errors, as shown above, although these systematic errors were comparable to the experimental errors in our system. If the experimental error is sufficiently small, e.g., 1–2%, these systematic errors can have serious consequences for subsequent motional analysis. To study CH vector motion in 15% ^{13}C-enriched nucleic acids, the following should be considered carefully: nondirectly bonded ^1H–^{13}C distances, underestimation of $^{13}C\{^1H\}$ NOE, the off-resonance contribution to $R(^{13}C_x)$ and $R(2^1H_z{}^{13}C_x)$, the base carbon CSA–DD cross-relaxation contribution to $R(2^1H_z{}^{13}C_z)$ and $R(2^1H_z{}^{13}C_x)$, and the proton–proton DD cross-relaxation contribution to $R(2^1H_z{}^{13}C_z)$.

Assessment of Relaxation Rates

Except for terminal residues, the observed relaxation rates for a given atom type showed no sequence-specific variation; i.e., the standard deviation of the relaxation rate values over the sequence was comparable to the average experimental error, ~5–10% (see Table S1 of Supplementary Materials placed at authors' website: http://picasso.ucsf.edu). Values for the transverse relaxation rates, $R(^{13}C_x)$ and $R(2^1H_z{}^{13}C_x)$, and the steady-state NOE were relatively scattered about the sequence. Significantly small or large values, which were defined by the averaged value and its standard deviation, were found for the following residues and positions; $R(^{13}C_x)$ (1′ of G11 and G20, 3′ of G11 and G20, 4′ of G11 and G20); $R(2^1H_z{}^{13}C_x)$ (1′ of G11, 3′ of G11 and G20, 4′ of G20); NOE (1′ of G11, 3′ of G11 and G20, 4′ of G11 and G20); $R(^{13}C_z)$ at 600 MHz (3′ of G20); $R(^{13}C_z)$ at 500 MHz (3′ of G20, 4′ of A12, 8 of A2); $R(2^1H_z{}^{13}C_z)$ at 600 MHz (3′ of G20); $R(2^1H_z{}^{13}C_z)$ at 500 MHz (1′ of G6 and A12); $R(^1H_z)$ at 600 MHz (3′ of A17); $R(^1H_z)$ at 600 MHz (1′ of G6, 3′ of G11, 8 of G6 and G20). In the above 11, 7, 6, 3, and 0 relaxation values were listed for the 3′, 1′, 4′, 8, and 2 positions, respectively. Values for sugar relaxation rates were relatively scattered. At base 2 position no significant deviations were detected, and at base 8 positions the error bar was too big to see any sequence dependence. Significantly different values were found for 11, 9, 3, 2, and 1 relaxation parameters for G20, G11, G6, A12, A2, and A17, respectively. Differences for the terminal residues, G11 and G20, might be expected. G6 and A12 could be special in motional and possibly structural character.

Differences in most relaxation rates depended more on chemical position than on position of the residue in the sequence. Most significant differences were found between sugar and base for many relaxation parameters. However, this difference could not be simply attributed to motional differences, since ^{13}C CSA values differed between sugar and base carbons. The proton-related relaxation rates, $R(^1H_z)$, $R(2^1H_z{}^{13}C_z)$ and $R(2^1H_z{}^{13}C_x)$, depended on chemical position. For example, at the adenine 2 position the proton longitudinal relaxation rate was very slow, but at the 3′ position it was relatively fast. The proton–proton dipolar auto-relaxation term ($\rho_{H^CH^i}$) reflects both proton densities and dynamics around proton H^C; as proton density clearly differs around each proton, variations in $\rho_{H^CH^i}$ could not be directly attributed to differences in dynamics.

CH Bond Length and ^{13}C Chemical Shift Anisotropy Values

Before applying Eq. [1], let us consider the CH bond length and the ^{13}C CSA values. The CH bond length (r_{CH}) is available from the literature. However, r_{CH} is not a physical constant; i.e., it depends on the chemical structure and the molecular conformation. For example, r_{CH} values of 1.090 ± 0.005 and 1.098 ± 0.007 Å, respectively, for the methyl and α positions

of amino acids (*66*), and 1.096 ± 0.005 and 1.084 ± 0.005 Å, respectively, for the aliphatic and aromatic positions of nucleotides (*41*) have been published. If vibrational averaging of the CH bond is considered, it becomes about 2% larger (*67, 68*). *Ab initio* molecular orbital calculations on β-D-ribofuranose suggest that sugar conformation affects the r_{CH} value within the 0.01 Å range (*69*). These studies suggest that a given r_{CH} value may have a 0.01 or a 0.02 Å error, so the relationship between r_{CH} and the motional parameters should be known. The order parameter S^2 is approximately scaled by the strength of the dipole–dipole interaction, which is proportional to the value D written in Eq. [1]. A 0.01 Å increase in the 1.09 Å CH distance corresponds to a 5.6% augmentation in the order parameter S^2 (*66*). In our system, S^2 was determined directly, thus affecting the bond length. The slope in the r_{CH} vs S^2 plot was 0.04 and 0.03 unit (5 and 4% increases) per 0.01 Å for sugar and base, respectively. It was smaller than expected (5.6%) due to the nonnegligible contribution from the CSA and internal motion. The fictitious decrease due to the non-directly bonded proton contribution, the 1% CH distance decrease corresponding to the 6% increase in the relaxation rate (*59*), should also be considered.In any case, the measured order parameter S^2 may have 0.03–0.05 unit uncertainty originating from ambiguity in CH bond length.

CSA values of sugar carbons were around 40 ppm (*42*), and the CSA contribution to relaxation of protonated carbons was nearly negligible. On the other hand, CSA values for purine base carbons have not been determined but are assumed to be relatively large. Principal elements of ^{13}C chemical shift tensors have been determined for more than 70 molecules (*70*), including 2′-deoxythymidine (*71*) and L-tryptophan (*72*), where $(\sigma_{11}, \sigma_{22}, \sigma_{33}) = (227, 122, 96), (242, 168, 89), (49, 130, 238), (202, 121, 48)$ in parts per million for C2, C4, C6 of dT and C2 of L-Trp, respectively. Assuming axial symmetry, the CSA value $\Delta = |\sigma_{\parallel} - \sigma_{\perp}|$ was around 120–150 ppm for dT and L-Trp, much smaller than the value of the toluene aromatic carbon (180 ppm) used in most ^{13}C relaxation studies of DNA (*14, 24, 28*). This overestimation can be a serious problem for determining motional parameters. In the present study, the order parameter S^2 was optimized, changing CSA values in 5-ppm steps from 110 to 185 ppm. The purpose of this calculation was to obtain the best quantitative estimation of the CSA contribution to the measured motional parameter (S^2 in this case) and to determine the most appropriate CSA values for purine ring carbons.

In Fig. 2, S^2 (○) and χ^2 (●) values are plotted against CSA values for C2 (upper) and C8 (lower). A linear function for S^2 and a parabolic function for χ^2 are shown by the fitted solid lines. The slopes of S^2 were -0.0028 and -0.0027 ppm^{-1} for C2 and C8, respectively, so the 10 ppm uncertainty in CSA values results in a 0.03 unit ambiguity in S^2. A similar relationship, altering CSA by ~20 ppm, changes S^2 by ~0.05 and has been reported for the aromatic ring carbons of the zinc-finger peptide Xfin-31 (*62*). The minimum χ^2 was obtained for CSA values of 161 and 150 ppm for C2 and C8, respectively. Our CSA values are much closer to those of the hetero-ring systems, dT and L-Trp, than to that of toluene. From a statistical view these values may have systematic errors, because our data set was measured at only two magnetic field strengths, and the number of samples was less than 10. However, as there was no compelling reason to use any dT, L-Trp, or toluene CSA values, 161 and 150 ppm for C2 and C8 were employed in subsequent calculations. We note that the 20–30 ppm increase in the CSA value by using the toluene CSA value (180 ppm) instead of our values (161 or 150 ppm) would lead to a 0.05–0.08 unit decrease in S^2.

Spectral Density Mapping

As described in Eq. [1], the spectral density mapping procedure can be applied to the six relaxation rates observed at 600 MHz. The three relaxation rates measured at 500 MHz, $R(^{13}C_z)$, $R(2^1H_z{}^{13}C_z)$, and $R(^1H_z)$, yielded only the spectral density value at 125 MHz, the ^{13}C frequency at 11.74 T. Thus the spectral density could be sampled at frequencies of 0, 125, 150, 450, 600, and 750 MHz in our analysis. The spectral density value at 0 MHz, $J_{eff}(0)$, included the exchange contribution as defined in Eq. [3]. Some negative spectral density values were found for $J(450)$ and $J(600)$, which is physically impossible. They could become positive if the large error were taken into account in those cases. The relative error increased with increasing monitoring frequency—about 5, 10, 10, 50, 100, and 50% at 0, 125, 150, 450, 600, 750 MHz, respectively. Essentially, the spectral density is a simple decay function, but the error was almost constant. The error in $J(600)$ was larger than others, because the $J(600)$ value was determined by five relaxation rates including the two transverse relaxation rates. The error in the transverse relaxation rates was relatively larger than the others, so the resulting errors for $J_{eff}(0)$, $J(600)$, and $\rho_{H^cH^i}$ were also larger since the transverse terms were substantial.

The spectral density values obtained may reflect all of the information from our relaxation data. However, motional information is limited for the target CH vector motion, and no motional model is available for the whole molecule. That is, the relationship between the spectral density values and the physical picture of the molecular motion is not clear. To clarify the situation somewhat, the correlation between any single spectral density value sampled at one frequency and each of the others was investigated. Though $J_{eff}(0)$ and $J(600)$ did not show any correlations, linear correlations were found for three combinations, $J(150)$–$J(450)$, $J(150)$–$J(750)$, and $J(450)$–$J(750)$. In Fig. 3, two negative correlations are plotted for $J(150)$ versus $J(450)$ (top) and $J(750)$ (bottom) with correlation coefficients of $R = 0.91$ and 0.93, respectively. The slopes and y-intercepts are -1.33 and 1.56×10^{-10} s/rad for $J(150)$–$J(450)$ and -0.22 and 2.88×10^{-11} s/rad for $J(150)$–$J(750)$, respectively. For $J(450)$–$J(750)$, the slope

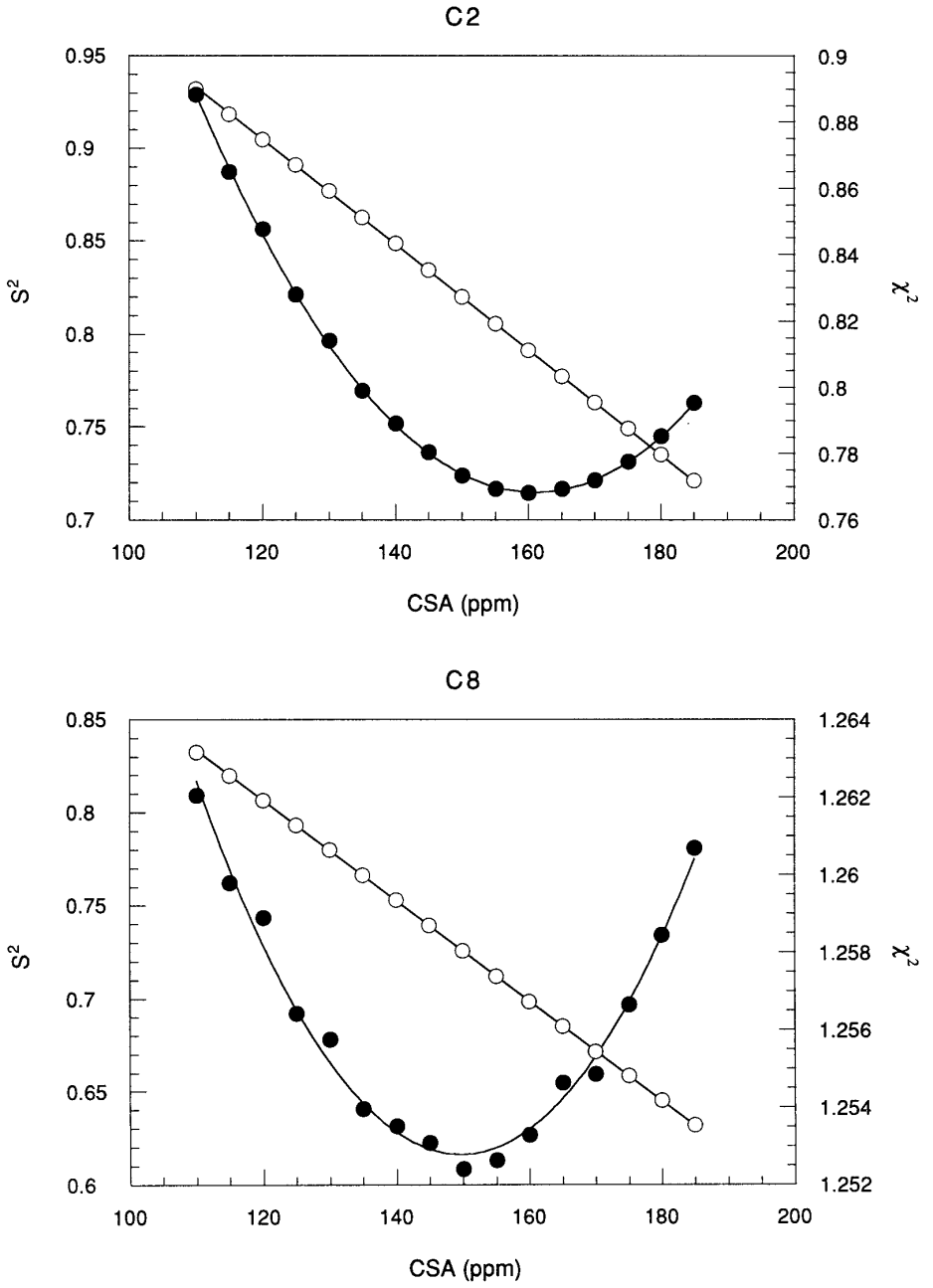

FIG. 2. The effect of the ^{13}C chemical shift anisotropy value $\Delta = |\sigma_{\|} - \sigma_{\perp}|$ of nuclei C2 (upper) and C8 (lower) on the generalized order parameter S^2 (○) and the root mean square of the χ^2 residuals (●), which are determined by the model-free calculations described in the text. With the overall correlation time kept at 3.30 ns, χ^2 was minimized to determine the model-free parameters, and the calculation was repeated every 5 ppm step for CSA values in the range 110–185 ppm. A linear function for S^2 and a parabolic function for χ^2 are shown by the fitted solid lines. The slopes of the S^2 lines are −0.0028/ppm for C2 and −0.0027/ppm for C8. χ^2 minima occurred at CSA values of 161 ppm for C2 and 150 ppm for C8.

and y-intercept are 0.15 and 3.81×10^{-12} s/rad ($R = 0.95$), respectively. The spectral density is a simple decay function, so positive slopes are expected. In fact, it is positive for $J(450)$–$J(750)$. The observed variation in spectral density values cannot be explained by a single correlation time, so at least two different motions must be required. The combination of a slower and a faster motion can account for the negative slopes. The reason is readily understood by using Eq. [5] as an example of a model-free approach. In Eq. [5], the total spectral density function consists of two terms which are related to the faster and slower motions, respectively. That is, the fractional contribution of the faster-motion term to the total spectral density increases with a decrease in that of the slower motion. This is a negative correlation. If the dominant motions on 150

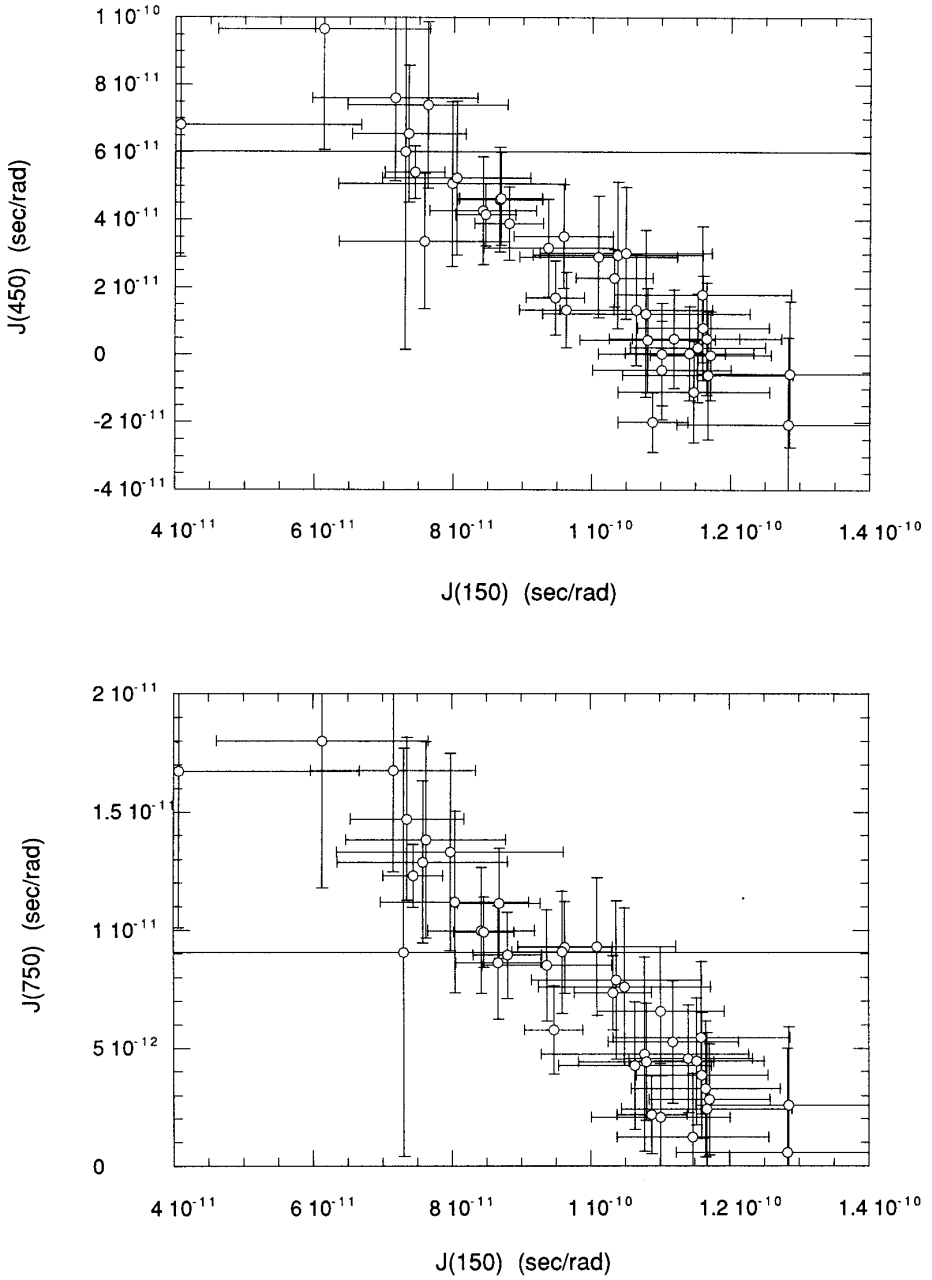

FIG. 3. Correlations among spectral density values at 150, 450, and 750 MHz. Two negative correlations are shown for $J(150)$ versus $J(450)$ (top) and versus $J(750)$ (bottom). A simple $y = ax + b$ function for this correlation yields correlation coefficients $R = 0.91$ and 0.93 for the $J(150)$–$J(450)$ and $J(150)$–$J(750)$ plots, and their slopes and y-intercepts are -1.33 and 1.56×10^{-10} for $J(150)$–$J(450)$ and -0.22 and 2.88×10^{-11} for $J(150)$–$J(750)$ plots, respectively. The resulting values of the two correlation times derived are 3.91 ns and 188 ps for the $J(150)$–$J(450)$ plot and 3.76 ns and 64 ps for the $J(150)$–$J(750)$ plot.

and 450 (or 750) MHz differ from each other, the resulting correlation becomes negative. At 450 and 750 MHz, the faster motion may be dominant, and at 150 MHz the slower motion may be dominant. If there are more than three motions, the situation becomes more complicated.

Previously, linear correlations between spectral density samplings at different frequencies have been noted in spectral density mapping analysis of the GAL4 protein (*73*). If the various motions are not correlated, the spectral density function $J(\omega)$ may be expressed by a linear combination of spectral density terms $J_i(\omega)$ characterizing each motion. This assumption is used in most motional models and analyses, including the anisotropic overall tumbling and model-free approaches. For example in Eq. [5], the first and second terms are assumed

to be the spectral density function of the overall and internal motions, respectively, where the order parameter S^2 and $(1 - S^2)$ scale the linear combination. The scaling factor varies on a residue-by-residue basis and chemical position-to-position basis, so each $J_i(\omega)$ component should obey the linear relationship

$$J_i(\omega_y) = \alpha J_i(\omega_x) + \beta, \quad [8]$$

where α and β are the slope and y-intercept. If the $J_i(\omega)$ components are given by a Lorentzian shape such as in Eq. [5], Eq. [8] results in a fourth degree equation in τ_{map},

$$5\beta\omega_x^2\omega_y^2\tau_{map}^4 + 2(\alpha\omega_y^2 - \omega_x^2)\tau_{map}^3 + 5\beta(\omega_x^2 + \omega_y^2)\tau_{map}^2 + 2(\alpha - 1)\tau_{map} + 5\beta = 0. \quad [9]$$

The four roots of Eq. [9] give the correlation times of the various motions, though this equation is hardly solved analytically. When a linear correlation is found such as Eq. [8], each motion may be characterized by a single correlation time. Therefore, the internal motion resulting in Eq. [5] should correspond to a unique correlation time for all residues and chemical positions. This is an important result, because we can count the number of motions by the number of real roots of Eq. [9]. If more than three real roots are found, Eq. [5] should be extended to treat additional motions correctly.

We used the mathematical software Mathematica 2.2 (Wolfram Research) to solve Eq. [9]. The resulting correlation times were 3.91 ± 0.37 ns and 188 ± 17 ps for $J(150)$–$J(450)$, 3.76 ± 0.29 ns and 64 ± 3 ps for $J(150)$–$J(750)$, and 2.74 ± 0.25 ns and 11 ± 1 ps for $J(450)$–$J(750)$. Two other solutions were imaginary for each, so only two motions are detectable for each data set. Errors were estimated by a Monte Carlo procedure as already described. The fitted parameters, slopes and y-intercepts, and their estimated errors were assumed to be the means and variances of Gaussian distributions. A hundred sets of the slope and y-intercept were created from these distributions and solved individually 100 times. The standard deviations of the resulting ensemble of correlation times were taken as the estimated errors. The difference of each correlation time was larger than the fitting errors, and five correlation times were found. However, this did not mean the presence of five apparent motions. As discussed above, the linear relationship of Eq. [8] did not allow any sequence-specific and atom site-specific variations for each correlation time. The two real roots of Eq. [9] correspond to two apparent motions, and their correlation times should be consistent for the three correlation plots (Fig. 3). Apparently, errors in the slope and y-intercept in the correlation plots (Fig. 3) or systematic errors in our experimental data were underestimated. However, it is also apparent that we can safely conclude that in our DNA duplex, two major motions exist with the slower and faster motions possessing correlation times of ~3–4 ns and ~10–200 ps.

Why did $J_{eff}(0)$ and $J(600)$ not show any correlations? Primarily, the absolute errors in $J_{eff}(0)$ and $J(600)$ were 2–5 times larger than the others, which is enough to mask any such correlation, especially for $J(600)$. Even for $J(150)$, $J(450)$, and $J(750)$, the error was large (Fig. 3). However, some correlation was expected for $J(0)$ because the absolute value of $J(0)$ was large; i.e., the relative error was small. In our case $J_{eff}(0)$ did not show any correlations with the other spectral density values, so the exchange term λR_{ex} in Eq. [3] is the likely cause. The exchange contribution can destroy correlations, because the magnitude of the exchange term is independent of the frequency which is the basis for the correlation of spectral density values. To estimate the magnitude of the exchange contribution in the spectral density mapping procedure, the magnetic field dependences of the six relaxation rates are required, which were not available in our study. Another explanation entails anisotropic overall tumbling. A change in the angle between the CH vector and the principal axes of the molecule evokes a change in the apparent tumbling rate; this affects mainly $J(0)$ and not the high-frequency terms of the spectral density. The exchange term and anisotropic overall tumbling will be reconsidered later.

In the above mapping analysis, Peng and Wagner's original method was used instead of reduced spectral density mapping (*34, 35*), because the reduced procedure will not enable us to investigate correlations between $J(150)$, $J(450)$, and $J(750)$. Reduced spectral density mapping has been proposed for determining spectral density values from ^{15}N T1, T2, and NOE values, because proton longitudinal, two spin-order longitudinal and transverse relaxation rates generally have some systematic errors. For protein ^1H–^{15}N, spectral density values of $J(\omega_H - \omega_N)$, $J(\omega_H)$, and $J(\omega_H + \omega_N)$ are similar each other, and 10 and 100 times smaller than $J(\omega_N)$ and $J(0)$, respectively. Thus either $J(\omega_H - \omega_N) = J(\omega_H) = J(\omega_H + \omega_N)$ or $J(\omega_H - \omega_N) = ((\omega_H - \omega_N)/\omega_H)^2 \times J(\omega_H) = ((\omega_H - \omega_N)/(\omega_H + \omega_N))^2 \times J(\omega_H + \omega_N)$ is assumed in the reduced mapping treatment. The former equation was based on $\omega\tau \ll 1$, but the latter equation was based on $J(\omega) \propto 1/\omega^2$, where $\omega\tau \gg 1$. These two equations give almost identical $J(0)$ and $J(\omega_N)$ values in the protein ^1H–^{15}N system (*34*). In our DNA ^1H–^{13}C system, the former equation was not suitable because the $J(450)$ values were ~2–3 times larger than $J(750)$ values. In the latter equation, $J(450)$ values were expected to be 2.8 times larger than $J(750)$ values, similar to our result. This suggests that the order parameter S^2 in Eq. [5] is large in our system. The former equation is appropriate for internal motion where $\omega\tau_i \sim 0.08$ for $\tau_i = 20$ ps at 600 MHz, but the latter is appropriate for overall motion where $\omega\tau_o \sim 12$ for $\tau_o = 3.3$ ns at 600 MHz. Note that values from complete spectral density mapping were required for all analyses of our DNA ^1H–^{13}C system.

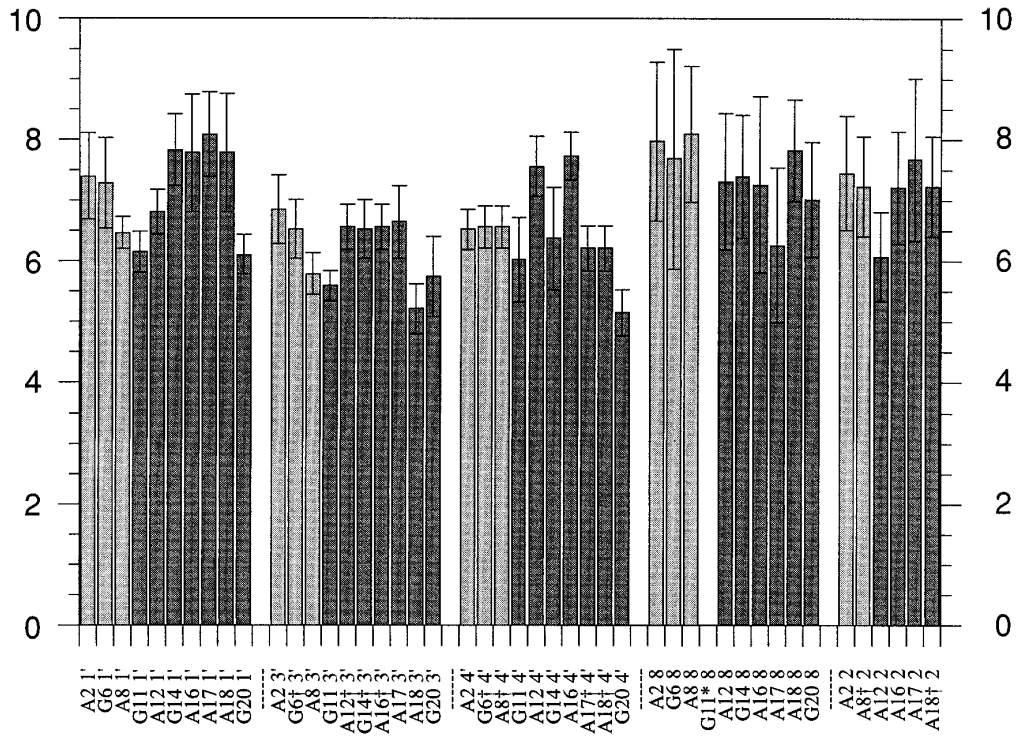

FIG. 4. Bar graph of the T1/T2 ratio $= R(^{13}C_x)/R(^{13}C_z)$ for ^{13}C nuclei in the decamer duplex, where $*$ and † designate missing or overlapping peaks, respectively (see Fig. 1). The different shading of the bars differentiates the duplex strands. The average T1/T2 ratio is 7.38 ± 0.54, 6.50 ± 0.31, 6.79 ± 0.55, 7.42 ± 0.56, and 7.13 ± 0.55 for 1′, 3′, 4′, 8, and 2, respectively. Base 8 and 2 positions had large ^{13}C CSA contributions. The isotropic correlation time τ_o = 3.30 ± 0.17 ns was determined by χ^2 residual minimization of the T1/T2 ratio assuming $S^2 = 1$.

Lipari–Szabo "Model-Free" Approach

For "model-free" analysis, the following information is required: a physical model for overall rotation, the number of the internal motions, and assumption of the exchange term λR_{ex} in Eq. [3]. These three aspects of information can be extracted from the spectral density mapping analysis or the T1/T2 ratio data. Generally the physical model of the overall motion is not given *a priori* but is estimated from the molecular shape. In our case, either isotropic tumbling or axially symmetric anisotropic tumbling may be applicable because the molecular shape of our DNA decamer is most conveniently considered to be a short cylinder (*11, 37, 74*). Model selection can be done by analysis of the ^{13}C T1/T2 ratio. The number of apparent motions is determined by the spectral density mapping analysis, and it is two in our case (*vide supra*). However, the number of internal motions is still unknown, because it depends on the physical model of the overall motion; e.g., the axially anisotropic overall tumbling model entails two correlation times associated with the apparent motion about the long and short molecular axes. If the overall motion is isotropic (or anisotropic), the number of the internal motions is consequently one (or zero) in our case. The conformational exchange term λR_{ex} also cannot be assumed *a priori*. The presence of the exchange term was suggested from the spectral density mapping analysis of our relaxation data (*vide supra*).

For analysis of the overall motion, values for the ^{13}C T1/T2 ratio $(= R(^{13}C_x)/R(^{13}C_z))$ were used because the T1/T2 ratio is approximately independent of internal motions (*20*). Shown in Fig. 4 is a bar graph of the ^{13}C T1/T2 ratio values observed as a function of chemical position and position in the DNA sequence, where $*$ and † indicate missing and overlapping peaks, respectively (see Fig. 1). Data from the two different strands of the duplex are distinguished by different shadings of the bars. From Fig. 4, it is apparent that the ^{13}C T1/T2 ratios are roughly identical regardless of position in the residue or the sequence, so isotropic tumbling was employed as an overall motion. For each carbon resonance, the T1/T2 ratio was calculated using $S^2 = 1$ in Eq. [5], and subjected to χ^2 minimization to determine the τ_o value. The overall correlation time τ_o was determined to be 3.30 ± 0.17 ns by averaging over all carbons, excluding the terminal residues where $R(^{13}C_z)$ values were significantly smaller than the others. When terminal residues were included in these calculations, the correlation time became 3.24 ± 0.21 ns. The averaged T1/T2 ratio was not converted to the correlation time, because the CSA contributions of sugar and base were different. The slower motion with correlation time of 3–4 ns, identified by spectral density mapping analysis, can reasonably be identified with the overall isotropic motion indicated by this "model-free" analysis. If the conformational exchange term λR_{ex} is considered explicitly,

the real T1/T2 ratio and the resulting correlation time could be smaller than the values ascertained here.

At each position, the averaged T1/T2 ratio was 7.38 ± 0.54, 6.50 ± 0.31, 6.79 ± 0.55, 7.42 ± 0.56, 7.13 ± 0.55, for C1′, 3′, 4′, 8, and 2, respectively, where terminal residues were excluded. The T1/T2 ratio was somewhat larger for 1′, 8, and 2 compared with that for the 3′ and 4′ positions. Though base 8 and 2 positions have large ^{13}C CSA contributions, this difference could be due to anisotropic overall tumbling. We can consider the possibility of anisotropic motion more carefully, as demonstrated in some protein ^{15}N relaxation analyses (*75–77*). Assuming a rigid cylindrically symmetric species the spectral density function $J(\omega)$ may be written as the sum of three Lorentzians (*78*),

$$J(\omega) = C_1 \frac{\tau_1}{1 + (\omega\tau_1)^2} + C_2 \frac{\tau_2}{1 + (\omega\tau_2)^2} + C_3 \frac{\tau_3}{1 + (\omega\tau_3)^2}, \quad [10]$$

where $C_1 = (1/4)(3\cos^2\theta - 1)^2$, $C_2 = 3\sin^2\theta\cos^2\theta$, $C_3 = (3/4)\sin^4\theta$, $\tau_1 = 1/(6D_\perp)$, $\tau_2 = 1/(D_\parallel + 5D_\perp)$, $\tau_3 = 1/(4D_\parallel + 2D_\perp)$, and θ = the polar angle between the cylindrical symmetry axis and the CH internuclear vector. $D_\parallel$ and $D_\perp$ are diffusion coefficients for rotation around the symmetry and transverse axes, respectively. The $D_\parallel/D_\perp$ ratio is governed by molecular shape: the analytical expressions are taken from the hydrodynamic model of Tirado, Lopez Martinez, and Garcia de la Torre (*79*), being appropriate for the range $2 \le p \le 30$, $D_\parallel/D_\perp = 4 * p^2/(11.523 * (1 + \delta_\parallel) * (\ln p + \delta_\perp))$, $\delta_\parallel = 1.119 * 10^{-4} + (0.6884/p) - (0.2019/p^2)$, $\delta_\perp = -0.662 + (0.917/p) - (0.050/p^2)$, where p is the ratio (L/d) of length (L) to diameter (d). The lower limit of p could be 1 ($1 \le p \le 30$) based on experimental results from the NMR and depolarized dynamic light scattering (*11*). For our DNA decamer duplex, $D_\parallel/D_\perp = 1.60, 1.55, 1.51$, assuming zero, one-half (1.6 Å), and one (3.2 Å) hydration shell, respectively. The ratio $\tau_1{:}\tau_2{:}\tau_3$ becomes 1:0.94–0.95:0.79–0.83, so these three correlation times cannot accommodate either the 3–4 ns slower motion or the 10–200 ps fast motion found in the spectral density mapping analysis. However, if most DNA molecules were stacked end to end, the $D_\parallel/D_\perp$ value could be much larger than 10, which would be sufficient to explain the different correlation times deduced. Considering further the possibility of this large $D_\parallel/D_\perp$ value, the polar angle θ was calculated from previously determined coordinates (*37*), i.e., 100.1° ± 11.7°, 71.5° ± 33.0°, 104.5° ± 27.2°, 80.9° ± 17.2°, and 96.4° ± 10.0° for the C1′, 3′, 4′, 8, and 2 positions, respectively. Most CH vectors aligned approximately perpendicular to the symmetry axis, but the CH vectors for 3′ and 4′ deviate more. If a CH vector is perpendicular to the molecular symmetry axis ($\theta = 90°$), $C_1 = \frac{1}{4}$, $C_2 = 0$, and $C_3 = \frac{3}{4}$. If parallel ($\theta = 0°$), $C_1 = 1$, and $C_2 = C_3 = 0$. τ_1 is always larger than τ_3 unless $D_\parallel/D_\perp \le 1$. Since the $|\theta - 90°|$ values at the 3′ and 4′ positions were larger than the others, slightly larger correlation times would be expected with $D_\parallel/D_\perp > 1$. Therefore, T1/T2 ratio values for 3′ and 4′ positions would be expected to be larger than those at the 1′, 8, and 2 positions. This theoretical consideration conflicts with the observed results, so the large $D_\parallel/D_\perp$ value is not realistic in our case. By χ^2 minimization of the T1/T2 ratio, on the contrary, a value of $D_\parallel/D_\perp = 0.71$ is obtained. That could in principle be related to dimerization via side-by-side interactions; however, the overall correlation time of about 3 ns is too small for a dimer of 40 nucleotides (~13 kDa). Consequently, there is no evidence to support the existence of anisotropic tumbling for our decamer duplex, although the shape is not spherical. The inability to detect anisotropic tumbling is largely due to the limits of experimental error and the alignment of the CH vector for the 1′, 3′, 4′, 8, and 2 positions perpendicular to the long axis (*vide supra*).

Three assumptions were employed in arriving at Eqs. [3] and [5] for the model-free calculation: isotropic overall tumbling, one internal motion, and the presence of the conformational exchange term λR_{ex}. The theoretical and experimental bases for these assumptions were discussed above. For the model-free parameter optimization, the overall correlation time was kept at 3.30 ns, which was determined by the T1/T2 ratio analysis. The other parameters, i.e., the internal correlation time τ_i, the order parameter S^2, the exchange contribution R_{ex} at 600 MHz, the proton–proton longitudinal relaxation rate $\rho_{H^cH^i}$ at 500 and 600 MHz, were optimized by χ^2 residual minimization as defined in Eq. [6]. The initial value of the internal motion correlation time τ_i was varied around 10–200 ps, which was found by the spectral density mapping analysis, to avoid falling into a local minimum of the χ^2 function. The measured order parameter S^2 is plotted in Fig. 5. Data from the two different strands of the duplex are distinguished by different shadings of the bars in the graph; the symbols * and † designate missing or overlapping peaks, respectively (see Fig. 1). From Fig. 5, it is apparent that, except for terminal residues, the order parameters S^2 are similar for most CH vectors. The average value is 0.79 ± 0.05 (0.77 ± 0.07) excluding (or including) terminal residues. The average fitting error was 0.04. Evidently, the scatter in values for the order parameter S^2 is principally explained by the fitting error. In Fig. 5, three larger values (A8 1′ = 0.87, A12 1′ = 0.92, A18 3′ = 0.91) and seven smaller values (G11 1′ = 0.69, G11 3′ = 0.66, G11 4′ = 0.68, A12 4′ = 0.70, A12 8 = 0.67, G20 3′ = 0.54, G20 8 = 0.62) were significantly different. Order parameter S^2 values for the A12 residue are scattered, and those of A8 1′ and A18 3′ are large. The smallest S^2 value is 0.54, for the 3′ position at the 3′ terminus (G20 3′). For terminal residues, the average S^2 was 0.67 ± 0.07. Note that no significantly different S^2 value is evident for G6, which has significantly larger or smaller relaxation rates.

The optimized internal motion correlation time τ_i is ~20 ps, which is consistent with the spectral density mapping analysis

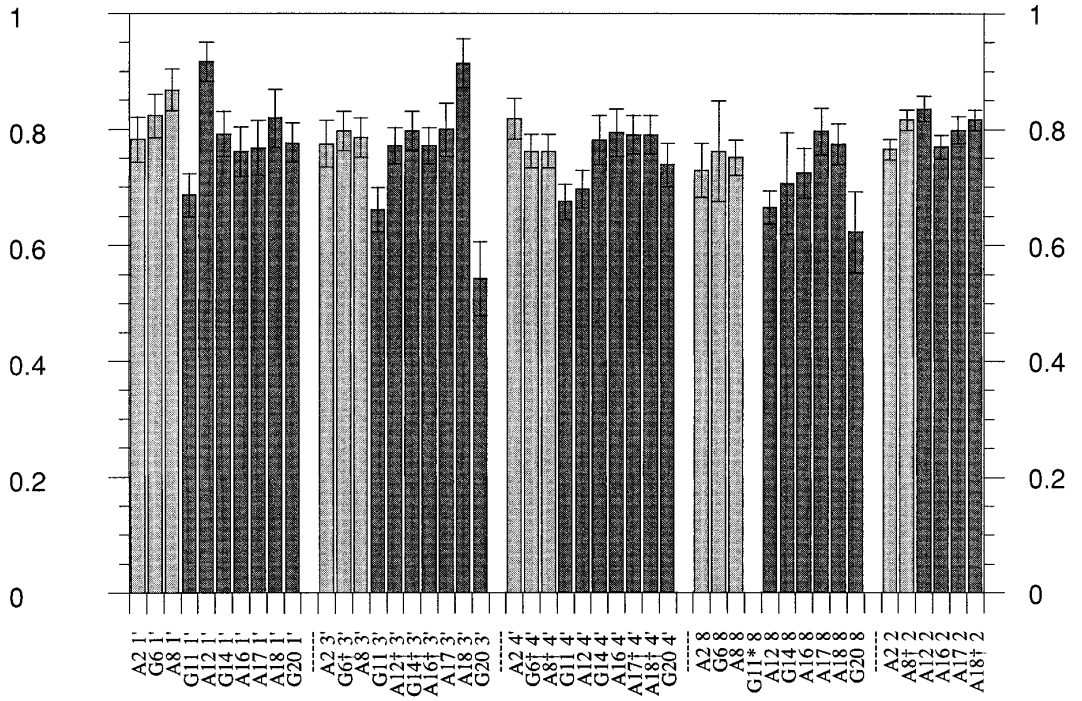

FIG. 5. Bar graph of the generalized order parameter S^2 for CH positions in the decamer duplex, where $*$ and † designate missing or overlapping peaks, respectively (see Fig. 1). The shading of the bars differentiates the two duplex strands. With the overall correlation time of 3.30 ns, the model-free parameters were determined by χ^2 residual minimization of nine relaxation parameters recorded at 500 and 600 MHz ^{1}H frequencies. The average order parameter S^2 was 0.79 ± 0.05.

results. This correlation time is not a well-defined parameter, as noted previously (*80*). The average value is 21 ± 16 ps, and the average fitting error is 19 ps (90% relative error). One negative value was obtained at the 8 position of G6 due to the very large relaxation rate error. The largest error was ± 64 ps; thus a comparison of values has no meaning except for terminal residues where the average τ_i value (45 ± 12 ps) was significantly larger than that of nonterminal residues.

The exchange contribution R_{ex} at 600 MHz is small, and the largest value is 2.6 Hz. The average value is 0.79 ± 0.72 Hz, and the average fitting error is 0.35 Hz (44% relative error). The value is quite scattered because for base and 1′ positions, it is larger than for 3′ and 4′; average values for each 1′, 3′, 4′, 8, and 2 position were 0.80, 0.17, 0.33, 1.56, and 0.69 Hz, respectively. Five negative values were found—at the A8 3′, G11 3′, A12 2, A18 3′, and G20 4′ positions. Most of them could be explained by the very large fitting error; however, at the A18 3′ position, it is clearly negative, strongly implying a systematic error in the transverse relaxation experiments or an incorrect fitting model. These R_{ex} values have a positive linear correlation (coefficient 0.69) with the corresponding $\{R(C_x) - R(C_z)/2\}$ values (*81*), where $\{R(C_x) - R(C_z)/2\} = 2E/3\ J(0) + 3D\ J(\omega_H) + R_{ex}$ (see Eq. [1]).

The proton–proton longitudinal relaxation rates $\rho_{H^cH^i}$ at 500 and 600 MHz clearly reveal position dependence. The order of $\rho_{H^cH^i}$ values is H3′ ~ 4′ ~ 8 > 1′ > 2 at 500 MHz, and 3′ > 4′ > 8 > 1′ > 2 at 600 MHz. This difference principally derives from the structure. These results will be considered later relative to the CORMA calculation. Average values (in rad/s) are 2.20 ± 0.82 and 2.39 ± 0.92, and average fitting errors are 0.18 and 0.16 (8% and 7% relative error) at 500 and 600 MHz, respectively. The $\rho_{H^cH^i}$ value at 600 MHz should be smaller than that at 500 MHz if the spectral density function $J(\omega)$ is a simple decay function. Our data did not obey that expectation, suggesting underestimation of the fitting error or systematic error in the experiments at either 500 or 600 MHz. The 500 MHz data were doubtful because of low S/N. From the magnitude of the relative error, the order parameter S^2 was the most precisely determined parameter (5% relative error), and the internal correlation time τ_i was the worst.

In many model-free calculations, three relaxation parameters (T1, T2, and NOE) have been used, since it is time-consuming to record and analyze more than three and the relaxation rates of the proton and the two-spin order coherence seemed to have some systematic errors. In our case, such errors were carefully suppressed to be <10%, which was approximately our experimental error. Three relaxation parameters enable determination of no more than three model-free parameters for each residue. However, for a more thorough analysis of the DNA duplex system, which has not been examined in detail previously, we deemed that the six relaxation rates would be required for the spectral density mapping and the T1/T2 ratio

analysis. For one thing, even the number of model-free parameters which should be considered was not known *a priori*. Our model-free calculation was based on three basic assumptions, i.e., isotropic overall tumbling, one internal motion, and the presence of the exchange term. These assumptions were examined via spectral density mapping analysis and T1/T2 ratio analysis, and required three model-free parameters. We found that three relaxation parameters sufficed. When three relaxation parameters were used for the model-free calculation of our DNA decamer, the model-free parameters determined were similar to those derived using nine relaxation parameters. However, the resulting model-free parameters were rather scattered and the fitting errors were about two times larger; consequently, the values from the analysis using three relaxation parameters were not employed in subsequent analyses. Additionally, if four or more model-free parameters were found to be required, it would be impossible to apply the method employing three relaxation parameters. If the spectral density mapping or the T1/T2 ratio analysis could not be trusted for some unexpected reason, our assumptions would become doubtful. Using nine relaxation parameters enabled several calculations to be carried out, based on different assumptions, to explore systematic errors in the analysis of DNA duplex dynamics via spectral density mapping and T1/T2 ratios. Possible effects from anisotropic overall motion, two internal motions, or absence of the exchange term could be tested. For each of these, there was no evidence to fault our basic assumptions.

CORMA Calculations

An alternative means of assessing proton–proton relaxation rates is available, since we have previously derived the time-averaged structure of the DNA decamer duplex which can be used as the basis for calculating interproton relaxation rates (*37*). Proton–proton dipolar auto- ($\rho_{H^cH^i}$) and cross-relaxation rates ($\sigma_{H^cH^i}$) were calculated using the program CORMA (COmplete Relaxation Matrix Analysis) (*82, 83*),which can account for parameters used in the model-free approach (*84*). For the CORMA calculation, the order parameter S^2 and the internal correlation time τ_i are required for each proton–proton vector. These parameters cannot be obtained rigorously from our current analysis, which focuses instead on proton–carbon vectors. The interproton vector parameters are not available even if ^1H–^1H NOESY data and ^1H–^{13}C (or ^1H–^{15}N) model-free parameters are combined. However, our model-free analysis indicates that the order parameter S^2 for CH vectors is $\sim$0.8 for the whole molecule, so the order parameter S^2 is also expected to be $\sim$0.8 for each proton–proton pair. Similarly, the internal motion correlation time τ_i of each proton–proton vector is assumed to be $\sim$20 ps. Other input data were the overall correlation time τ_o, 3.30 ns, the proton resonance frequency, 600 MHz, and the atomic coordinates (*37*). Auto-relaxation rates as well as the sum of cross-relaxation rates were calculated for each proton to estimate systematic errors in $R(2^1H_z{}^{13}C_z)$ and $R(2^1H_z{}^{13}C_x)$ which can occur due to the proton–proton cross-relaxation; for that systematic error, see Relaxation Rate Measurements, above.

The auto-relaxation rates calculated from CORMA (CORMA data set) were compared with two experimental values determined by different methods, i.e., from spectral density mapping (mapping data set) and from the model-free approach (model-free data set). The $\rho_{H^cH^i}$ values of the CORMA and mapping data sets were in the range 0–6 rad/s, but those of the model-free data set were systematically smaller (0–3 rad/s). No clear correlation was expected because the experimental error of the mapping data set was 20–80%, 4–8 times larger than that of the model-free data set. Although not strong, a somewhat positive correlation was found among all of them. Since $\rho_{H^cH^i}$ values strongly depend on position, the average value for each position should be a good indicator with which to compare data sets. The average values, excluding terminal residues, are listed in Table S1 (of the Supplementary Materials) for all three data sets. The values are similar for H3′ protons, but not for the others, especially H8. The mapping data set gave values relatively larger than the others. The standard deviation was large for both H8 and H2 of the mapping data set and for H8 of the CORMA data set. The order was well conserved, except for H8: H8 > H3′ > H4′ > H1′ > H2 (CORMA data set), H8 > H3′ > H4′ > H1′ > H2 (mapping data set), and H3′ > H4′ > H8 > H1′ > H2 (model-free data set). For H8, significantly larger values were obtained in the CORMA and mapping data sets, although nonselective ^1H T1 values of the non-labeled sample were about 2.0–2.3 s for all H1′, H3′, H4′, and H8 (*36*). For a further detailed comparison, the CORMA data set should be refined using a conformational ensemble procedure (*4, 8, 85*) or a very reliable molecular dynamics (MD) simulation, e.g., incorporating the particle mesh Ewald (PME) method (*86*). Indeed, long molecular dynamics simulations with PME are currently being conducted on the same DNA duplex as studied here (*87*).

Motion of the DNA Decamer Duplex

The spectral density mapping method of Peng and Wagner and the model-free approach of Lipari and Szabo provide substantial information about motion, e.g., spectral density values at several frequencies, overall and internal motion correlation times, and site-specific values of the order parameter S^2. Information derived from the different approaches could generally be rationalized by some simple assumptions. Here we validate our assumptions and exceptions to yield a consistent picture of the motion for our DNA decamer.

When axially symmetric tumbling of DNA as a cylinder, instead of isotropic tumbling, was employed, the order parameter S^2 and the χ^2 value increase with increasing ratio of the

rotational diffusion coefficients $D_{\|}/D_{\perp}$. For the DNA decamer, the upper limit to $D_{\|}/D_{\perp}$ might expected to be 1.5–1.6 from the molecular shape, but isotropic tumbling with $D_{\|}/D_{\perp} = 1$ gave the smallest χ^2 value. Two reasonable conclusions present themselves: either isotropic overall tumbling is a suitable motional model or any existing anisotropic motion was not detected. Most CH vectors at 1′, 3′, 4′, 8 and 2 positions are approximately perpendicular to the helix axis—the symmetry axis—and the direction of the various different 3′ and 4′ CH vectors can be easily affected by small differences in sugar conformation and motions. Consequently, there was no substantial evidence either to support or to deny the possible existence of anisotropic motion. When anisotropic tumbling with $D_{\|}/D_{\perp} = 1.51$–1.60 is assumed, the effective isotropic correlation time $(2D_{\|} + 4D_{\perp})^{-1}$ becomes about 3% larger than the value determined for the isotropic correlation time, 3.30 ns.

When the exchange term was omitted in fitting the relaxation data, the χ^2 value drastically increased (~50%). However, if the overall correlation time τ_o was optimized individually for each CH vector in the absence of the exchange term, the resulting τ_o, S^2, and χ^2 increased about 10%, 1%, and 1%, respectively. The χ^2 value obviously did not change much, implying that the effect of the exchange term is principally reflected in a change in τ_o value. In other words, it was difficult to distinguish slow motions from exchange broadening contributions to the $J(0)$ value in our analysis. When two internal motions were assumed instead of one (*88*), the derived order parameters and internal motion correlation times did not converge to realistic values for more than half of the residues. Assuming the absence of an exchange term and setting the fast internal motion correlation time to 20 ps, about half of the residues had reasonable values similar to that obtained assuming only one internal motion, but the χ^2 values were still not small. A distribution of the internal motion correlation time was also considered (*59*) but the χ^2 minimization was not successful due to the very fast internal motion. We note as well that slow internal motion is not independent of anisotropic overall tumbling in the numerical fitting of relaxation parameters; i.e., when $D_{\|}/D_{\perp} \geq 1.3$ and anisotropic overall tumbling occurs, it can be rationalized as isotropic motion with a nonexistent slow internal motion (*89*). Judging from χ^2 values and the convergence of the model-free parameters, our basic assumptions appear to be more reasonable than other assumptions and models.

In the model-free calculation discussed above, χ^2 values did not change much, either including or excluding an exchange term, as long as the overall correlation time τ_o was fitted independently for each residue. Spectral density mapping provides a different perspective on exchange. If exchange exists, the $J(0)$ values determined from the spectral density mapping are actually $J_{\text{eff}}(0)$ as shown in Eq. [3]. As exchange terms were determined from the model-free calculation, these exchange terms could be subtracted from $J_{\text{eff}}(0)$ to yield a corrected $J(0)$, $J_{\text{cor}}(0)$. As discussed above, some correlation (positive or negative) would be expected between $J(0)$ and the other spectral density values. The correlation coefficients between $J_{\text{cor}}(0)$ and $J(150)$, $J(450)$, and $J(750)$ were 0.70, −0.51, and −0.57, respectively, while correlation coefficients between $J_{\text{eff}}(0)$ and the others were 0.29, 0.07, and −0.25, respectively. Clear correlations were found for $J_{\text{cor}}(0)$, but not for $J_{\text{eff}}(0)$. The positive correlation of $J_{\text{cor}}(0)$–$J(150)$ and two negative correlations of $J_{\text{cor}}(0)$–$J(450)$ and $J_{\text{cor}}(0)$–$J(750)$ are consistent with the previous conclusion that the overall motion is dominant at 150 MHz and the internal motion is dominant at 450 and 750 MHz. Exchange effects in principle should be manifest in additional line broadening, but that could not be demonstrated by our experimental data because our transverse relaxation data were recorded only at 600 MHz without pulse field dependence. Consequently, the time scale of these exchange terms cannot be firmly established. For example, our analysis indicates that slow or very slow internal motions are acceptable as a source of the exchange terms. The large exchange terms were found at 1′ and base positions, together with larger $\rho_{H^cH^i}$ values at the base 8 position. Thus, the presence of substantial motion around the glycosidic bond (χ angle), as would occur for base pair opening (*90*), *syn–anti* equilibrium interconversion (*42*), or large χ angle libration (*3*) could explain the exchange term, although the time scale is unknown. Evaluation of the time scale of the large exchange term is currently in progress by ^{1}H and ^{13}C $T_{1\rho}$ experiments.

The amplitude of the motion is defined by the order parameter S^2, and the correlation time gives us the apparent frequency of the motion. However, the order parameter S^2 is an abstract number and only experientially related to the concept of rigid or flexible. The average order parameter value S^2 for our DNA decamer is 0.79 ± 0.05, a value similar to that of a well-structured protein core, ~0.8–0.9. In other words, our DNA decamer is as rigid as a typical protein. To give a physical image to the order parameter S^2, the diffusion-in-a-cone model (*31*) provides a simple example: $S^2 = 0.25 \cos^2\theta (1 + \cos\theta)^2$, and θ = the angle of the cone. When $S^2 = (1, 0.90, 0.80, 0.70, 0.60, 0.50, 0)$, $\theta = (0°, 15.1°, 21.9°, 27.5°, 32.7°, 37.8°, 90°)$, respectively. If $0.85 \geq S^2 \geq 0.25$, S^2 and θ are linearly correlated by $S^2 = -0.019\theta + 1.22$. The average order parameter $S^2 = 0.79$ corresponds to $\theta = 22.5°$, which would generally be considered as fairly restricted motion. The smallest value we found, $S^2 = 0.54$, corresponds to $\theta = 35.8°$; it is comparatively flexible but still restricted. Apparently, the motion of our DNA decamer was quite restricted over the whole molecule; no CH vector was freely moving even at the terminal residues. Strictly, this conclusion pertains to all of the purine residues which we had labeled, but it is likely to hold in general.

While our analysis was perhaps more thorough, our con-

clusions are strongly consistent with and preceded by the studies of other groups on DNA or RNA double helix regions (*6*, *29*, *91*). For example, the average order parameter S^2 at the 1′ position of a DNA 11-mer was 0.80 ± 0.09 including pyrimidine nucleotides but excluding terminal residues (*29*). The order parameter S^2 of a self-complementary DNA octamer was also about 0.8 (*6*). Even for ΔTAR RNA 29-mer, it was concluded that S^2 values at the 6 and 8 positions on the bases were 0.7–0.9 in the stem region although ^{13}C enrichment was >95% and neighboring carbon and proton contributions to the relaxation rates were neglected (*91*) Also of note, the order parameters S^2 of intraresidue ^1H–^1H vectors computed from the molecular dynamics trajectory of a DNA octamer were in the range 0.7–0.9 (*92*). The examples above also manifest some variations (ca.: 0.05–0.1) depending on the sequence, which were comparable to our experimental errors.

Solid-state ^2H NMR studies tell us that the amplitude of a fast local motion was in the order C8–^2H < C6–^2H < C2–$^2H''$ < C5–$^2H'$ for the ^2H-labeled DNA duplex *d*(CGCGAATTCGCG)$_2$ (*18*). In solution, the initial buildup rates of NOESY cross-peaks of the sugar H2′–H2″ and cytosine H5–H6 are explained by assuming the identical correlation time for sugar and base in *d*(CGCGAATTCGCG)$_2$ (*17*) and in *d*(CGTACG)$_2$ (*15*), which is qualitatively inconsistent. Although the precision of the solution data is not very high, for comparison of these data, Lane calculated the semiangles for motion within a cone (*12*). The amplitude of the fast internal motion is low for both base and sugar and for both solution and solid state. However, most amplitudes in solution are larger than those in the solid state. Due to the low precision of the data, a detailed comparison may not be meaningful, but a somewhat enhanced flexibility in the solution state is apparent. In our solution state analysis, no difference in motional properties was evident for the sugar 1′, 3′, 4′ and base 8, 2 positions. However, we did not derive motional parameters for sugar 2′ and 5′ positions where higher mobility is expected (*6*, *13*, *16*), so details of the sugar motion were not characterized in this report.

Although most values of the order parameter S^2 deviated little from 0.8 in our study, there were exceptions: those from different A12 CH vectors were scattered, and S^2 values for A8 1′ and A18 3′ were large. The exchange contribution R_{ex} of A18 3′ was even negative. A12 and A18 residues are not terminal (G11, G20) nor at kinked positions (G6, A8, G14, A16), so structural peculiarities will not readily account for the exceptions. Assuming two internal motions without the exchange term (*88*), an S^2 value of 0.70 was obtained for A18 3′ although the χ^2 value was slightly larger than that for the one internal motion model; this treatment did not work well for A8 1′ and A12 residues. The fraction of major *S*-type sugar conformer (%*S*) of our DNA decamer was previously determined from proton–proton scalar coupling constants (*36*). Both A8 and A18 residues exhibited lower fractions of *S* conformer, 0.76 and 0.82, respectively, than all others (~0.95) except terminal residues. This suggests that the A8 and A18 residues may possess additional motion associated with sugar repuckering. The fraction of the major sugar conformer correlates with $J_{eff}(0)$, the T1/T2 ratio, and the exchange contribution R_{ex} for sugar resonances. In Fig. 6, the relationship between the sugar conformation fractions and $J_{eff}(0)$ values are plotted for 1′, 3′, and 4′ positions within the sequence. The $J_{eff}(0)$ values were obtained by spectral density mapping. The $J_{eff}(0)$ values of 1′ are systematically large. While we have explained it by the presence of the slow motion and the exchange contribution term R_{ex}, there is another possible explanation. If the sugar carbon CSA values are assumed to be $1' > 4' \geq 3'$, the large $J_{eff}(0)$ values of 1′ can be explained without motional aspects. For example, the 0.1–0.2 ns/rad difference in $J_{eff}(0)$ seen between 1′ and 3′ (4′) can result if the CSA value of 1′ carbon is 80–110 ppm, not 40 ppm. Individual measured CSA values of sugar carbons would be required to establish details in sugar motion.

As for sequence-specific variations, a qualitative correlation between %*S* and $J_{eff}(0)$ is evident in Fig. 6. However, no obvious correlation was found between %*S* and the order parameter S^2. For example, while the smaller S^2 values were related to smaller %*S* values for the terminal residues, G11 and G20, residues A8 and A18 had somewhat larger S^2 values but their %*S* values were smaller. Of course, a rationalization may lie in the different time scales involved: the fractional conformer populations may entail conformer interconversion on a time scale as slow as milliseconds, but the order parameter reflects motions on a time scale as small as nanoseconds. When an explicit exchange term was assumed, the observed T1/T2 ratio = $(T1/T2)_0 + T1 \times R_{ex}$, where $(T1/T2)_0$ is the T1/T2 ratio excluding exchange. If T1 were similar for each and the overall motion were isotropic, a linear correlation between the exchange term and the T1/T2 ratio would be expected; a positive correlation coefficient of 0.74 was found. $J_{eff}(0)$ values also manifested a positive correlation coefficient of 0.76 with the T1/T2 ratio, because the overall motion is dominant for both $J_{eff}(0)$ and the T1/T2 ratio. The three qualitative correlations between sugar conformational equilibria and $J_{eff}(0)$, the T1/T2 ratio, and the exchange contribution R_{ex} were numerically consistent with each other. However, the correlation of a larger exchange term with a larger fraction of *S* conformer is not readily understood. We would judge that any changes in $J_{eff}(0)$ and the T1/T2 ratio should not be explained by the exchange term R_{ex} for A8, G11, A18, and G20 residues if the smaller *S* fraction was related to greater motion. Obviously, our analyses cannot explain everything, especially for the A8, A12, and A18 residues. However, the qualitative correlation found between the fraction of *S*-type sugar conformation and $J_{eff}(0)$ and the T1/T2 ratio suggests the pres-

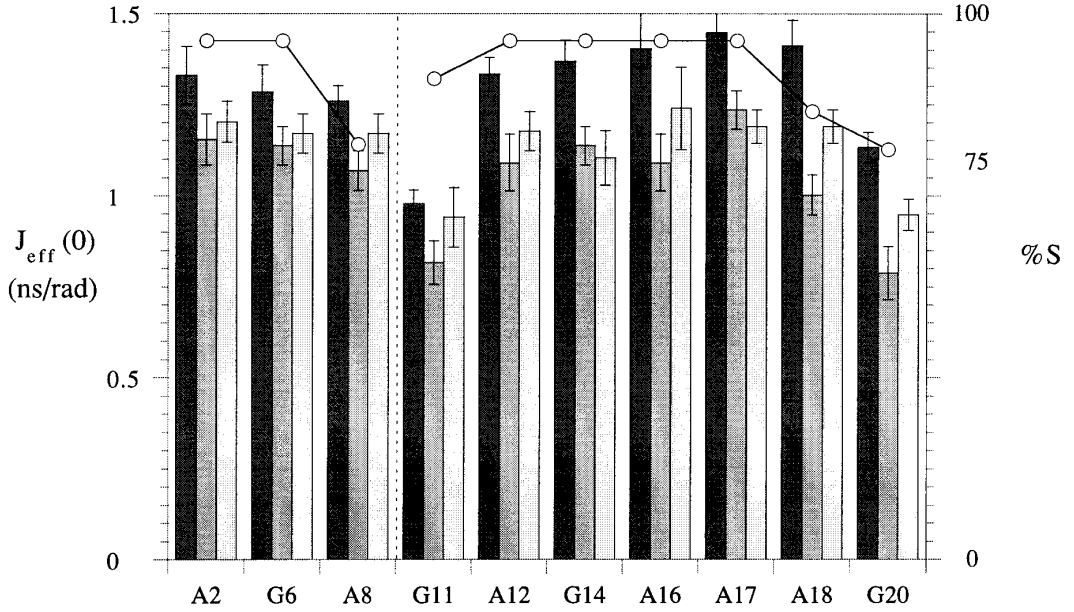

FIG. 6. The relationship between the fraction of 2′-*endo* (*S*-type) sugar conformation (%*S*) as previously determined (*36*) (—○—) and the effective $J(0)$ values at positions 1′, 3′, and 4′ as a function of position in the DNA sequence. The effective $J(0)$ values, $J_{eff}(0)$, were obtained via spectral density mapping. The bars represent $J_{eff}(0)$ values for 1′ (darker), 3′ (medium), and 4′ (lighter).

ence of a motion related to the sugar conformational equilibrium or repuckering motion.

CONCLUSIONS

A careful ^{13}C relaxation study has been carried out on the DNA decamer duplex, *d*(CATTTGCATC) · *d*(GATGCAAATG), in which every adenosine and guanidine residue was chemically enriched with 15% ^{13}C and 98% ^{15}N stable isotopes. Nine ^{13}C relaxation parameters were determined for CH spin systems of deoxyribose 1′, 3′, 4′ and base 8, 2 positions within 5–10% experimental error: $R(^{13}C_z)$, $R(^{1}H_z)$ and $R(2^{1}H_z{}^{13}C_z)$ were measured at both 500 and 600 MHz (^1H frequency), and $R(^{13}C_x)$, $R(2^{1}H_z{}^{13}C_x)$, and steady-state ^{13}C–^1H NOE were measured at 600 MHz. A dependence of relaxation parameters on chemical position was clearly observed; however, no sequence-specific variation was readily evident except for 3′ and 5′ termini. From theoretical and experimental considerations, it was demonstrated that the random 15% ^{13}C enrichment effectively suppressed both scalar and dipolar contributions of the neighboring carbons and protons on the relaxation parameters. We examined several potential complicating factors which could lead to systematic errors. In general, the following problematic issues should be considered carefully: non-directly bonded short ^1H–^{13}C distances, underestimation of $^{13}C\{^1H\}$ NOE, the off-resonance contribution to $R(^{13}C_x)$ and $R(2^{1}H_z{}^{13}C_x)$, the CSA–DD cross-relaxation contribution to $R(2^{1}H_z{}^{13}C_z)$ and $R(2^{1}H_z{}^{13}C_x)$ for base carbons, and the proton–proton dipolar cross-relaxation contribution to $R(2^{1}H_z{}^{13}C_z)$. In analysis for our system, we found that most of them were comparable to the random experimental errors. For most CH systems in the labeled decamer duplex with randomly fractionally 15% ^{13}C-enriched purine nucleotides, ^{13}C relaxation parameter values were reliably determined.

The full spectral density mapping introduced by Peng and Wagner and the model-free approach promulgated by Lipari and Szabo were applied to assess all observed relaxation parameters in a complementary manner. Spectral density mapping exhibited a linear correlation between three spectral density values, $J(\omega_C)$, $J(\omega_H - \omega_C)$, and $J(\omega_H + \omega_C)$ in plots containing all measured values, but not for the other spectral density terms including $J(0)$. These linear correlations reflect the effect of overall motion and similar internal motions for each CH vector in the decamer. Lack of correlations entailing $J(0)$ imply that relatively slow chemical exchange contributes to yielding effective $J_{eff}(0)$ values. Assuming a Lorentzian lineshape for $J(\omega)$, the slopes and *y*-intercepts of these correlation plots yielded two correlation times, 3–4 ns and 10–200 ps, which evinced the presence of two apparent motions. The first value, 3–4 ns, corresponds to the value of 3.3 ns obtained for the overall isotropic tumbling correlation time determined from analysis of ^{13}C T1/T2 ratios. The possibility of anisotropic overall tumbling was examined, but statistical analysis indicated a better fit to experimental data with the basic assumption of isotropic tumbling, probably due to the relative alignment of CH vectors and the level of experimental error. Based on spectral density mapping and the T1/T2 ratio analysis, three

basic assumptions were initially employed for the model-free calculation: isotropic overall tumbling, one internal motion, and the presence of chemical exchange terms. The order parameter S^2 and the corresponding fast internal motion correlation time were determined to be about 0.8 ± 0.1 and 20 ± 20 ps, respectively, for the various CH vectors. For terminal residues, values for the order parameter S^2 were slightly smaller, 0.5–0.8. No clear differences in S^2 were found between or within sugars and bases. The exchange term was small (<3 Hz) but explicit. In this DNA decamer, the internal motion was very fast (ps–ns time scale) and its amplitude was restricted, e.g., assuming a simple wobble-in-a-cone model, the internal motion was restricted to an angular amplitude of $\pm 22.5°$ for each of the 1′, 3′, 4′, 2, and 8 positions in the purine nucleotides in the entire duplex. This is in contrast to the flexible DNA phosphodiester backbone (*5*).

We examined the effect of structural parameters, specifically, CH bond length and chemical shift anisotropy, on motional parameters derived from our analyses. CSA values of base C2 and C8 were optimized via χ^2 residual minimization (Eq. [6], yielding values of 161 and 150 ppm, respectively. A 20–30 ppm increase in CSA value, using the toluene CSA value (180 ppm) instead of our optimized values (161 or 150 ppm), would lead to a 0.05–0.08 unit decrease in S^2. The dependence of the order parameter S^2 on the CH bond length was found to be 0.04 and 0.03 unit per 0.01 Å for sugar and base, respectively. If vibrational averaging of the CH bond is important, the CH bond length could be slightly larger (0.01–0.02 Å) than the value of 1.09 Å used in the analysis, suggesting that the measured order parameters S^2 could be slightly larger, ~0.05 unit. Systematic errors arising from uncertainties in the CSA and the CH bond length are off-setting and comparable to the fitting error or the standard deviation of the scatter, ~0.05. The exceptions, S^2 values for the A12 residue, A8 1′, and A18 3′, were not explained very well, possibly due to inappropriate assumptions or a motional model. It may be noteworthy that for A8 and A18 residues, the fraction of 2′-*endo* (*S*-type) sugar conformation (%*S*) was previously found to be lower than that for other residues While the %*S* value had no clear relationship with the S^2 value for A8, A18, and terminal residues, a qualitative correlation was observed between the %*S* value and the effective $J(0)$ and T1/T2 ratio values. For further analysis of sugar motions, experimental determination of exact $J(0)$ values and the exchange contribution term R_{ex} will be required at all sugar CH positions, including 2′.

ACKNOWLEDGMENTS

We thank the Central Research Laboratories of Ajinomoto Co., Inc., for assistance in preparing isotope-labeled adenosine and guanosine. We also acknowledge Dr. Shin-Ichi Tate (Tokyo Metropolitan University) for showing us his unpublished relaxation data of 15% ^{13}C-labeled DNA. This work was supported by Grant RG401/95 from the Human Frontier Science Program (Strasbourg, France) and Grant GM39247 from the National Institutes of Health to T.L.J., and by a grant from CREST (Core Research Evolutional Science and Technology) of Japan Science and Technology Corporation (JST) to M.K. C.K. was supported in part by a Toyobo Biotechnology Foundation and JSPS Fellowship.

Supporting Information Available

We are placing the following information at our website: http://picasso.ucsf.edu. Three tables and one figure (five pages): the observed relaxation rates and T1/T2 ratios (Table S1), the spectral density function values sampled at six frequencies (Table S2), the model-free parameters (Table S3), and the plot of the spin-lock pulse sequence dependence on the ^{13}C transverse relaxation rate (Fig. S1). We will also deposit information, as appropriate, with the BioMagResBank (http://www.bmrb.wisc.edu).

REFERENCES

1. S. S. Wijmenga, M. M. W. Mooren, and C. W. Hilbers, *in* "NMR in Macromolecules" (G. C. Roberts, Ed.), pp. 217–288, IRL Press, Oxford (1993).
2. U. Schmitz and T. L. James, *Methods Enzymol.* **261,** 3–44 (1995).
3. M. Tonelli and T. L. James, *Biochemistry* **37,** 11478–11487 (1998).
4. N. B. Ulyanov, U. Schmitz, A. Kumar, and T. L. James, *Biophys. J.* **68,** 13–24 (1995).
5. T. L. James, *in* "Phosphorus-31 NMR. Principles and Applications" (D. Gorenstein, Ed.) pp. 349–400, Academic Press, New York (1984).
6. A. N. Lane, *Methods Enzymol.* **261,** 413–435 (1995).
7. D. A. Pearlman, *J. Biomol. NMR* **4,** 1–16 (1994).
8. U. Schmitz, A. Kumar, and T. L. James, *J. Am. Chem. Soc.* **114,** 10654–10656 (1992).
9. B. H. Robinson and G. P. Drobny, *Methods Enzymol.* **261,** 451–509 (1995).
10. D. P. Millar, *Curr. Opin. Struct. Biol.* **6,** 322–326 (1996).
11. W. Eimer, J. R. Williamson, S. G. Boxer, and R. Pecora, *Biochemistry* **29,** 799–811 (1990).
12. A. N. Lane, *Prog. NMR Spectrosc.* **25,** 481–505 (1993).
13. A. N. Lane, *Carbohydr. Res.* **221,** 123–144 (1991).
14. P. N. Borer, S. R. LaPlante, A. Kumar, N. Zanatta, A. Martin, A. Hakkinen, and G. C. Levy, *Biochemistry* **33,** 2441–2450 (1994).
15. A. N. Lane and M. J. Forster, *Eur. Biophys. J.* **17,** 221–232 (1989).
16. P. Koehl and J.-F. Lefevre, *J. Magn. Reson.* **86,** 565–583 (1990).
17. B. Reid, K. Banks, P. Flynn, and W. Nerdal, *Biochemistry* **28,** 10001–10007 (1989).
18. T. M. Alam, J. Orban, and G. Drobny, *Biochemistry* **30,** 9229–9237 (1991).
19. N. R. Nirmala and G. Wagner, *J. Am. Chem. Soc.* **110,** 7557–7558 (1988).
20. L. E. Kay, D. A. Torchia, and A. Bax, *Biochemistry* **28,** 8972–8979 (1989).
21. J. W. Peng and G. Wagner, *J. Magn. Reson.* **98,** 308–332 (1992).

22. D. R. Muhandiram, T. Yamazaki, B. D. Sykes, and L. E. Kay, *J. Am. Chem. Soc.* **117,** 11536–11544 (1995).
23. T. Yamazaki, R. Muhandiram, and L. E. Kay, *J. Am. Chem. Soc.* **116,** 8266–8278 (1994).
24. J. R. Williamson and S. G. Boxer, *Nucleic Acids Res* **16,** 1529–1540 (1988).
25. E. R. Kellenbach, M. L. Remerowski, D. Eib, R. Boelens, G. A. van der Marel, H. van den Elst, J. H. van Boom, and R. Kaptein, *Nucl. Acids Res.* **20,** 653–657 (1992).
26. G. Lancelot, L. Chanteloup, J.-M. Beau, and N. T. Thuong, *J. Am. Chem. Soc.* **115,** 1599–1600 (1993).
27. T. Sekine, E. Kawashima, and Y. Ishido, *Tetrahedron Lett.* **37,** 7757–7760 (1996).
28. J. R. Williamson and S. G. Boxer, *Biochemistry* **28,** 2819–2831 (1989).
29. F. Paquet, F. Gaudin, and G. Lancelot, *J. Biomol. NMR* **8,** 252–260 (1996).
30. A. J. Wand, J. L. Urbauer, R. P. McEvoy, and R. J. Bieber, *Biochemistry* **35,** 6116–6125 (1996).
31. R. E. London, *Methods Enzymol.* **176,** 358–375 (1989).
32. G. Lipari and A. Szabo, *J. Am. Chem. Soc.* **104,** 4546–4559 (1982).
33. J. W. Peng and G. Wagner, *Biochemistry* **34,** 16733–16752 (1995).
34. N. A. Farrow, O. Zhang, A. Szabo, D. A. Torchia, and L. E. Kay, *J. Biomol. NMR* **6,** 153–162 (1995).
35. R. Ishima and K. Nagayama, *J. Magn. Reson. B* **108,** 73–76 (1995).
36. K. Weisz, R. H. Shafer, W. Egan, and T. L. James, *Biochemistry* **31,** 7477–7487 (1992).
37. K. Weisz, R. H. Shafer, W. Egan, and T. L. James, *Biochemistry* **33,** 354–366 (1994).
38. V. A. Daragan, M. A. Kloczewiak, and K. H. Mayo, *Biochemistry* **32,** 10580–10590 (1993).
39. A. Abragam, "Principles of Nuclear Magnetism," Oxford Univ. Press, Oxford (1961).
40. R. R. Ernst, G. Bodenhausen, and A. Wokaun, "Principles of Nuclear Magnetic Resonance in One and Two Dimensions," Clarendon Press, Oxford (1987).
41. W. Saenger, "Principles of Nucleic Acid Structure," Springer-Verlag, New York (1984).
42. F. Gaudin, F. Paquet, L. Chanteloup, J. M. Beau, T. T. Nguyen, and G. Lancelot, *J. Biomol. NMR* **5,** 49–58 (1995).
43. M. Akke and A. G. Palmer III, *J. Am. Chem. Soc.* **118,** 911–912 (1996).
44. S. Tate, A. Ono, and M. Kainosho, *J. Am. Chem. Soc.* **116,** 5977–5978 (1994).
45. E. Nikonowicz, A. Sirr, P. Legault, F. M. Jucker, L. M. Baer, and A. Pardi, *Nucleic Acids Res.* **20,** 4507–4513 (1992).
46. M. J. Michnicka, J. W. Harper, and G. C. King, *Biochemistry* **32,** 127–136 (1993).
47. M. J. Robins, J. S. Wilson, and F. J. Hansske, *J. Am. Chem. Soc.* **105,** 4059–4065 (1983).
48. T. Atrinson, and M. Smith, *in* "Oligonucleotide Synthesis: A Practical Approach" (M. J. Gait, Ed.), pp. 349–400, IRL Press, Oxford (1984).
49. Y. Kyogoku, C. Kojima, S. J. Lee, H. Tochio, N. Suzuki, H. Matsuo, and M. Shirakawa, *Methods Enzymol.* **261,** 524–541 (1995).
50. J. D. Puglisi and I. Tinoco, Jr., *Methods Enzymol.* **180,** 304–325 (1989).
51. S. W. Fesik and E. R. P. Zuiderweg, *J. Magn. Reson.* **78,** 588–593 (1988).
52. D. Marion, M. Ikura, R. Tschudin, and A. Bax, *J. Magn. Reson.* **85,** 393–399 (1989).
53. K. Takegoshi, K. Ogura, and K. Hikichi, *J. Magn. Reson.* **84,** 611–615 (1989).
54. F. Delaglio, S. Grzesiek, G. W. Vuister, G. Zhu, J. Pfeifer, and A. Bax, *J. Biomol. NMR* **6,** 277–293 (1995).
55. R. A. Santos, P. Tang, and G. S. Harbison, *Biochemistry* **28,** 9372–9378 (1989).
56. M. Tomasz, J. Olson, and C. M. Mercado, *Biochemistry* **11,** 1235–1241 (1972).
57. P. Legault and A. Pardi, *J. Am. Chem. Soc.* **119,** 6621–6628 (1997).
58. M. J. P. v. Dongen, S. S. Wijmenga, R. Eritja, F. Azorin, and C. W. Hilbers, *J. Biomol. NMR* **8,** 207–212 (1996).
59. P. Allard, J. Jarvet, A. Ehrenberg, and A. Graslund, *J. Biomol. NMR* **5,** 133–146 (1995).
60. J. W. Peng and G. Wagner, *Methods Enzymol.* **239,** 563–596 (1994).
61. L. E. Kay, L. K. Nicholson, F. Delaglio, A. Bax, and D. A. Torchia, *J. Magn. Reson.* **97,** 359–375 (1992).
62. A. G. Palmer III, R. A. Hochstrasser, D. P. Miller, M. Rance, and P. E. Wright, *J. Am. Chem. Soc.* **115,** 6333–6345 (1993).
63. V. Sklenar, D. Torchia, and A. Bax, *J. Magn. Reson.* (1987).
64. A. G. Palmer III, N. J. Skelton, W. J. Chazin, P. E. Wright, and M. Rance, *Mol. Phys.* **75,** 699–711 (1992).
65. D. G. Davis, M. E. Perlman, and R. E. London, *J. Magn. Reson. B* **104,** 266–275 (1994).
66. L. K. Nicholson, L. E. Kay, and D. A. Torchia, *in* "NMR Spectroscopy and Its Application to Biomedical Research" (S. K. Sarkar, Ed.) pp. 241–279, Elsevier Science B.V., Amsterdam (1996).
67. L. M. Jackman and J. C. Trewella, *J. Am. Chem. Soc.* **98,** 5712–5714 (1976).
68. R. L. Vold, R. R. Vold, and D. Canet, *J. Chem. Phys.* **66,** 1202–1216 (1977).
69. C. A. Podlasek, W. A. Stripe, I. Carmichael, M. Shang, B. Basu, and A. S. Serianni, *J. Am. Chem. Soc.* **118,** 1413–1425 (1996).
70. W. S. Veeman, *Prog. NMR Spectrosc.* **16,** 193–235 (1984).
71. D. M. Gregory, M. A. Mehta, J. C. Shiels, and G. P. Drobny, *J. Chem. Phys.* **107,** 28–42 (1997).
72. F. Separovic, K. Hayamizu, R. Smith, and B. A. Cornell, *Chem. Phys. Lett.* **181,** 157–162 (1991).
73. J.-F. Lefèvre, K. T. Dayie, J. W. Peng, and G. Wagner, *Biochemistry* **35,** 2674–2686 (1996).
74. J. M. Withka, S. Swaminathan, and P. H. Bolton, *J. Magn. Reson.* **89,** 386–390 (1990).
75. R. Brüschweiler, X. Liao, and P. E. Wright, *Science* **268,** 886–889 (1995).
76. N. Tjandra, S. E. Feller, R. W. Pastor, and A. Bax, *J. Am. Chem. Soc.* **117,** 12562–12566 (1995).
77. Z. Zheng, J. Czaplicki, and O. Jardetzky, *Biochemistry* **34,** 5212–5223 (1995).
78. D. E. Woessner, *J. Chem. Phys.* **37,** 647–654 (1962).
79. M. M. Tirado, M. C. Lopez Martinez, and J. Garcia de la Torre, *J. Chem. Phys.* **81,** 2047–2052 (1984).

80. J. Q. Yu, D. S. Blumenthal, and P. N. Borer, *J. Chem. Inf. Comput. Sci.* **35,** 803–805 (1995).

81. I. Q. H. Phan, J. Boyd, and I. D. Campbell, *J. Biomol. NMR* **8,** 369–378 (1996).

82. J. W. Keepers and T. L. James, *J. Magn. Reson.* **57,** 404–426 (1984).

83. B. A. Borgias and T. L. James, *J. Magn. Reson.* **79,** 493–512 (1988).

84. A. Kumar, T. L. James, and G. C. Levy, *Israel J. Chem.* **32,** 257–261 (1992).

85. D. A. Pearlman, *J. Biomol. NMR* **4,** 279–300 (1994).

86. T. E. Cheatham III, J. L. Miller, T. Fox, T. A. Darden, and P. A. Kollman, *J. Am. Chem. Soc.* **117,** 4193–4194 (1995).

87. D. E. Konerding, T. E. Cheatham III, P. A. Kollman, and T. L. James, *J. Biomolec. NMR,* in press.

88. G. M. Clore, A. Szabo, A. Bax, L. E. Kay, P. C. Driscoll, and A. M. Gronenborn, *J. Am. Chem. Soc.* **112,** 4989–4981 (1990).

89. J. M. Schurr, H. P. Babcock, and B. S. Fujimoto, *J. Magn. Reson. B* **105,** 211–224 (1994).

90. M. Guéron and J. L. Leroy, *Methods Enzymol.* **261,** 383–413 (1995).

91. G. C. King, J. W. Harper, and Z. Xi, *Methods Enzymol.* **261,** 436–450 (1995).

92. T. M. G. Koning, R. Boelens, G. A. van der Marel, J. H. van Boom, and R. Kaptein, *Biochemistry* **30,** 3787–3797 (1991).